arXiv:1401.2667v3 [gr-qc] 5 May 2014

Static detectors and circular-geodesic detectors on the Schwarzschild black hole

Lee Hodgkinson[1*] , Jorma Louko[1†] and Adrian C. Ottewill[2‡]

[1] *School of Mathematical Sciences,*
University of Nottingham, Nottingham NG7 2RD, UK

[2] *School of Mathematical Sciences and Complex & Adaptive Systems Laboratory,*
University College Dublin, UCD, Belfield, Dublin 4, Ireland

(Revised March 2014)

Published in Phys. Rev. D **89**, 104002 (2014)

Abstract

We examine the response of an Unruh-DeWitt particle detector coupled to a massless scalar field on the (3+1)-dimensional Schwarzschild spacetime, in the Boulware, Hartle-Hawking and Unruh states, for static detectors and detectors on circular geodesics, by primarily numerical methods. For the static detector, the response in the Hartle-Hawking state exhibits the known thermality at the local Hawking temperature, and the response in the Unruh state is thermal at the local Hawking temperature in the limit of a large detector energy gap. For the circular-geodesic detector, we find evidence of thermality in the limit of a large energy gap for the Hartle-Hawking and Unruh states, at a temperature that exceeds the Doppler-shifted local Hawing temperature. Detailed quantitative comparisons between the three states are given. The response in the Hartle-Hawking state is compared with the response in the Minkowski vacuum and in the Minkowski thermal state for the corresponding Rindler, drifted Rindler, and circularly accelerated trajectories. The analysis takes place within first-order perturbation theory and relies in an essential way on stationarity.

*lee.hodgkinson@nottingham.ac.uk
†jorma.louko@nottingham.ac.uk
‡adrian.ottewill@ucd.ie

1 Introduction

The Unruh-DeWitt detector [1, 2] is a simple model particle detector — a two-state quantum-mechanical system coupled to the quantum field. As we shall see, the particular quantum-mechanical system chosen is unimportant; however, the reader may find it helpful to keep in mind a concrete picture of the detector as, say, a two-state hydrogen atom.

On a curved spacetime or for non-inertial observers, the particle content of the field is ambiguous, and a distinguished notion of a "particle", defined with respect to some timelike Killing vector, may not exist. Unruh-DeWitt detectors liberate us from the reliance on symmetries to investigate particle content, and they provide an operational definition of the field's particle content. The tool of Unruh-DeWitt detectors has been applied in several situations, which include accelerated observers in Minkowski spacetimes [1, 2, 3, 4, 5, 6, 7], static detectors in exterior Schwarzschild [8, 9], inertial detectors in de Sitter space [10], and static, co-rotating and freely-falling detectors on the Bañados-Teitelboim-Zanelli (BTZ) black hole [11].

To study an Unruh-DeWitt detector in a given spacetime, we use first-order perturbation theory, and we are led to the notions of the detector response function and the instantaneous transition rate. Heuristically, the detector response function gives the probability of a transition between the states of the detector, and the transition rate represents the "number of particles detected per unit proper time". The transition rate will be the primary quantity of interest in this paper. In general, one must take extreme care in obtaining the response function and transition rate [12, 13, 14, 15]; sufficient conditions are that the quantum state of the field is regular in the Hadamard sense [16, 17] and that the detector is switched on (off) smoothly [18, 19, 20, 21].

However, in this paper we shall be concerned with stationary detectors for which the initial state of the field is invariant under the timelike Killing vector that generates the trajectory, and owing to this, the switch-on of the detector can be pushed to the infinite past and the transition rate is time-independent, within first-order perturbation theory. In this case, we can bypass the sensitive issues of regularisation and switching by integrating formally over the whole trajectory and factoring out the infinite total proper time integral [22].

In this paper, we use numerical methods to solve the radial part of the Klein-Gordon equation for a massless scalar field on four-dimensional Schwarzschild spacetime. We investigate static detectors and also detectors on circular geodesics (stable or unstable) in the exterior region, and we consider the Hartle-Hawking, Boulware and Unruh states for the field.

For the static detector in the Hartle-Hawking state, the response is known to be thermal [8] in the Kubo-Martin-Schwinger (KMS) sense [23, 24] — the local Hawking temperature at radial coordinate $R > 2M$ is equal to $T_{\rm loc} = T_H(1 - 2M/R)^{-1/2}$, where $M > 0$ is the mass of the black hole and $T_H = (8\pi M)^{-1}$ is the asymptotic temperature at infinity [25, 26]. Our numerical calculation provides the detailed profile of this thermal response, including the factors due to the density of states on the curved background [27].

For the circular-geodesic detectors in the Hartle-Hawking and Unruh states, we find evidence that the detector responds thermally in the limit of a large energy gap, at a temperature higher than that recorded by the static detector, by a factor larger than the time dilation Doppler shift factor. We show analytically that the same phenomenon occurs for a stationary detector in three qualitatively similar situations in Minkowski spacetime. The physical explanation for the blueshift exceeding time dilation appears to be that the transition rate at large excitation energies is dominated by the most energetic field quanta, and these are seen by the detector from a head-on direction and are hence blueshifted more than just by time dilation. This explanation is consistent with the analysis of a circular-geodesic detector in [28] within a model in which the angular dependence of the field is suppressed, where the asymptotic temperature in a state closely resembling the Unruh state was found to be related to the local Hawking temperature by just the time dilation Doppler shift factor.

We see no qualitative difference between the transition rates of stable versus unstable circular orbits.

For both the static and circular-geodesic detectors, we find that the Boulware and Unruh rates align at negative detector energy gap when the distance from the hole is large. This is consistent with the Unruh state mimicking an outgoing flux of radiation from a collapsing star that diminishes as r^{-2} and the fact that the Boulware state reduces to the Minkowski vacuum at spatial infinity. Similarly, because of this property of the Unruh state and the fact the Hartle-Hawking state represents a thermal bath at infinity, we see that the ratio of the excitation part of the transition rate in the Hartle-Hawking state to the transition rate in the Unruh state becomes large as the radius increases.

Considering the static detector, as the magnitude of the energy gap is increased further, all three states align for large negative energies. For both the static and circular-geodesic detectors, we see that at large magnitude energy gaps, the transition rate becomes oscillatory when the detector is near the horizon; this effect is due to back-scattering by the effective potential induced by the curvature. It is reminiscent of the oscillation observed for the BTZ black hole in [11], and we verify analytically that similar oscillations

take place also in Minkowski space for a field with an external potential barrier.

For the static detector with the field in the Boulware state, we see that the transition rate has a vanishing excitation rate (only de-excitation), and this is consistent with the fact that for a static trajectory we are on an orbit of the Schwarzschild time-translation Killing vector. Whereas for the circular detector with the field in the Boulware state, the transition rate now has a small excitation component due to synchrotron radiation [4], and this component gets smaller as the radius from the hole increases — consistent with the fact the circular detector is asymptotically static.

When the field is in the Unruh state, we find that the transition rate of the static and circular-geodesic detectors at a given radius remains non-vanishing even in the limit of a vanishing excitation energy. This may at first seem surprising: one may expect that such low-frequency modes in the outgoing flux, which the Unruh state simulates, would not be able to escape the gravitational potential. We address these concerns by verifying the non-vanishing result analytically.

We investigate the analogy between a uniformly linearly accelerated detector coupled to a field in the Minkowski vacuum in flat spacetime with the static detector in the Hartle-Hawking state on the Schwarzschild black hole, finding that the transition rates in the two cases align — the agreement becoming better as the radius increases. Similarly, for the circular-geodesic detector a comparison between its transition rate and that of a Rindler detector given a transverse drift velocity is analysed, and we find good agreement as the radius increases. Making the drift direction periodic does not, however, improve the agreement.

The plan of the paper now follows. In Section 2 we give an overview of the Unruh-DeWitt detector model, introducing the usual notion of a transition rate for stationary situations within first-order perturbation theory. In Section 3 we recall relevant features of the massless Klein-Gordon equation in four-dimensional Schwarzschild spacetime: in particular, we present in Section 3.1 our numerical scheme to solve the radial equation under the appropriate boundary conditions and in Section 3.2 our procedure for normalising the numerical solutions. Section 4 presents the mode sum expressions for the Wightman function in the Hartle-Hawking state, the Boulware state and the Unruh state. Section 5 presents the mode sum expressions for the transition rate for a static detector in each of these tree quantum states, and Section 6 presents the similar mode sum expressions for a detector on a circular geodesic. Section 7 sets up the analytic framework for comparing the static and circular-geodesic detectors in Schwarzschild to detectors in Rindler space, respectively on worldlines of uniform linear acceleration and

on worldlines of uniform linear acccleration with a transverse drift.

The numerical results are presented and analysed in Section 8. Section 9 gives a summary and concluding remarks. The three appendices analyse respectively the small energy behaviour of the Schwarzschild radial mode functions, a static detector coupled to a field with an external potential barrier in Minkowski spacetime, and a detector in Minkowski spacetime in stationary situations where there is a nonvanishing drift velocity with respect to thermally responding detectors.

Our metric signature is $(-+++)$. We use units in which $c = \hbar = k_B = 1$, so that frequencies, energies and temperatures have dimension inverse length. The Schwarzschild mass parameter is denoted by M and has dimension length. Spacetime points and Lorentz four-vectors are denoted with sans-serif letters (x), and Euclidean three-vectors are denoted with bold letters ($\mathbf{x}$). For the Minkowski or Euclidean product of two vectors of the respective kind we use a dot notation, $\mathsf{x} \cdot \mathsf{x}$ or $\mathbf{x} \cdot \mathbf{x}$.

2 Unruh-DeWitt detectors in static or stationary settings

In this section, we give a brief overview of the Unruh-DeWitt detector model [1, 2]. The Unruh-DeWitt detector is an idealised 'atom'; it is spatially point-like and comprises two states: $|0_d\rangle$, which has energy 0, and the state $|E_d\rangle$, which has energy E, where E may be a positive or negative real number.

The detector moves through spacetime on the trajectory $\mathsf{x}(\tau)$, where τ is the detector's proper time. This simple quantum-mechanical system (detector) is coupled to a real, free, scalar, quantum field, ϕ, by the interaction Hamiltonian

$$H_{\text{int}} = c\chi(\tau)\mu(\tau)\phi(\mathsf{x}(\tau)) \,, \tag{2.1}$$

where c is a small coupling-constant, χ is known as the switching-function and μ is the monopole-moment operator of our 'atom'. We can think of the switching function χ as turning on (off) our detector; in other words, as χ goes to zero the detector and field are decoupled, so no particles in the field are detected. In a general situation, we would now emphasise the necessity of χ being smooth and of compact support, but in the case of trajectories that are generated by the timelike Killing vectors of the spacetime, this requirement can be relaxed.

During the course of the detector's motion through spacetime, the detector will absorb (emit) quanta of energy, (de-)exciting it from its initial state to alternative state. The first question we must address is "what is the

probability of such a transition occurring?" We answer this question within the framework of first-order perturbation theory.

We shall assume the field is initially in some arbitrary Hadamard state [16]. Hadamard states have many desirable properties. In a Hadamard state, the stress-energy tensor is guaranteed to be renormalisable, and the singularity structure of the Wightman function in the coincidence limit is well defined [16]. All the states considered in this paper (Hartle-Hawking, Boulware and Unruh states on the Schwarzschild black hole) are Hadamard states.

We shall denote this initial Hadamard state of the field as $|\Psi\rangle$, and before the interaction begins, we assume the detector to be in the state $|0\rangle_d$. The detector-field system is, hence, initially in the composite state $|0\rangle_d \otimes |\Psi\rangle$. Regardless of the final state of the field, we are interested in the probability for the detector to be found in the state $|E\rangle_d$ after the interaction has ceased. Working in first-order perturbation theory, this probability factorises as [22, 29]

$$P(E) = c^2 |{}_d\langle 0|\mu(0)|E\rangle_d|^2 \mathcal{F}(E) \ , \tag{2.2}$$

where the response function $\mathcal{F}(E)$ encodes the information about the detector's trajectory, the initial state of the field and the way the detector has been switched on and off. $\mathcal{F}(E)$ can be expressed as

$$\mathcal{F}(E) = \lim_{\epsilon \to 0_+} \int_{-\infty}^{\infty} \mathrm{d}\tau' \int_{-\infty}^{\infty} \mathrm{d}\tau'' \, \chi(\tau')\chi(\tau'') \, \mathrm{e}^{-iE(\tau'-\tau'')} \, W_\epsilon(\tau', \tau'') \, , \tag{2.3}$$

where $W_\epsilon(\tau', \tau'')$ is a one-parameter family of functions that converge to the pull-back of the Wightman distribution on the detector's worldline [14, 16, 18, 19]. The factors in front of $\mathcal{F}(E)$ in (2.2) depend only on the internal structure of the detector and we shall from now on drop them, referring to $\mathcal{F}(E)$ as the transition probability.

If we restrict the motion of the detector to be along the orbit of a timelike Killing vector, and we assume $|\Psi\rangle$ to be invariant under the isometry generated by this Killing vector, the Wightman function is time-translation invariant along the trajectory, and we are free to push the switch-on time of the detector to the asymptotic past — effectively replacing the switching-function χ by the Heaviside step-function. With a change of variables, the result is that we can formally just drop the external τ'-integral of (2.3) in order to obtain the *transition rate* [22]:

$$\dot{\mathcal{F}}(E) = \lim_{\epsilon \to 0_+} \int_{-\infty}^{\infty} \mathrm{d}s \, \mathrm{e}^{-iEs} \, W_\epsilon(s) \, . \tag{2.4}$$

The transition rate represents the number of particles detected per unit proper time (this interpretation is slightly simplistic, see [14]), and it will be the primary quantity of interest throughout this paper.

3 Schwarzschild antecedents

In four-dimensional Schwarzschild spacetime, the Wightman function is not known analytically, and in this section we present the numerical methods necessary to study the transition rate of a detector coupled to a massless, minimally-coupled, scalar field in the Hartle-Hawking, Boulware and Unruh states.

The metric of the Schwarzschild spacetime is given by

$$ds^2 = -\left(1-\frac{2M}{r}\right)dt^2 + \left(1-\frac{2M}{r}\right)^{-1}dr^2 + r^2\left(d\theta^2+\sin^2\theta d\phi^2\right)\,, \quad (3.1)$$

where we assume the mass parameter M to be positive, the black hole exterior is covered by $2M < r < \infty$, and the horizon is at $r \to 2M$.

Mode solutions of the Klein-Gordon equation in the Schwarzschild spacetime have the form [22]

$$\frac{1}{\sqrt{4\pi\omega}} r^{-1}\rho_{\omega\ell}(r)Y_{\ell m}(\theta,\phi)\,\mathrm{e}^{-i\omega t}\,, \quad (3.2)$$

where $\omega > 0$, $Y_{\ell m}$ is a spherical harmonic and the radial function $\rho_{\omega\ell}$ satisfies

$$\frac{d^2\rho_{\omega\ell}}{dr^{*2}} + \left\{\omega^2 - \left(1-\frac{2M}{r}\right)\left[\frac{\ell(\ell+1)}{r^2}+\frac{2M}{r^3}\right]\right\}\rho_{\omega\ell} = 0\,, \quad (3.3)$$

with r^* being the tortoise co-ordinate, defined as

$$r^* = r + 2M\log\left(r/2M-1\right). \quad (3.4)$$

Alternatively, one can work with the Schwarzschild radial co-ordinate r and define the function $\phi_{\omega\ell}(r) := \rho_{\omega\ell}(r)/r$, which satisfies

$$\phi''_{\omega\ell}(r) + \frac{2\left(r-M\right)}{r\left(r-2M\right)}\phi'_{\omega\ell}(r) + \left(\frac{\omega^2 r^2}{(r-2M)^2} - \frac{\lambda}{r(r-2M)}\right)\phi_{\omega\ell}(r) = 0\,, \quad (3.5)$$

with $\lambda := \ell(\ell+1)$. Solutions to neither (3.3) nor (3.5) can be found analytically, and as such we seek the solutions $\phi_{\omega\ell}(r)$ numerically using code written in Mathematica (TM) [30].

In the asymptotic limit of $r \to \infty$, equation (3.5) has solutions $\phi(r) \approx \mathrm{e}^{\pm i\omega r*}/r$. The mode solutions with the simple form $\mathrm{e}^{+i\omega r*}/r$ as the leading order term at infinity are known as 'up-modes', and despite being of this simple outgoing form at infinity they are a linear superposition of ingoing and outgoing modes at the horizon. Conversely, we have mode solutions known as 'in-modes' that take on a simple ingoing form at the horizon, $\mathrm{e}^{-i\omega r*}/r$, but because of scattering from the potential term in (3.3) they are a linear superposition of ingoing and outgoing modes at infinity. The up- and in-modes are illustrated schematically in Figure 1.

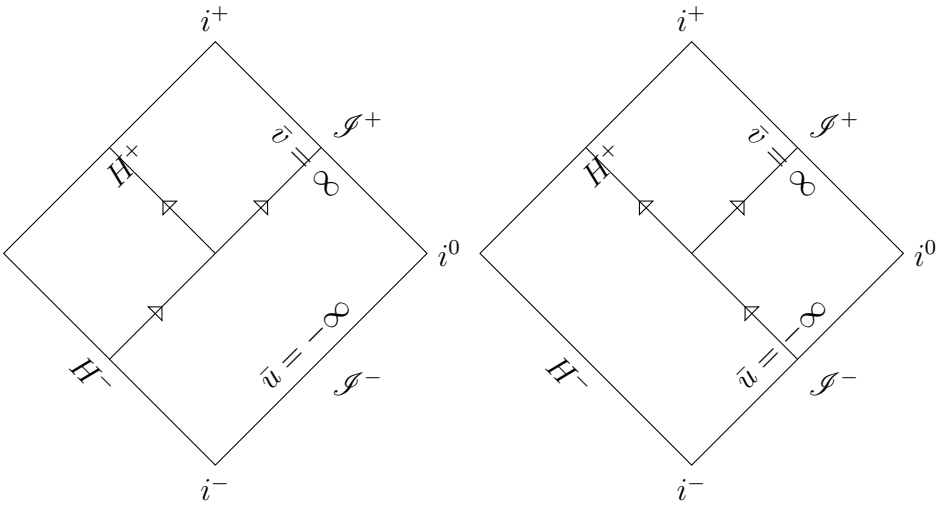

Figure 1: Illustrating the 'up' and 'in' modes on the right-hand wedge of the Penrose diagram representing the region exterior to the four-dimensional Schwarzschild black hole. The 'up' modes are shown on the left-hand side and 'in' modes on the right-hand side.

3.1 Numerical methods for obtaining the boundary conditions

Our first task is to find boundary conditions for both the in-modes and up-modes. With these boundary conditions for $\phi^{\rm in}_{\omega\ell}, \phi^{\rm up}_{\omega\ell}$ and $\phi^{\rm in}{}'_{\omega\ell}, \phi^{\rm up\prime}_{\omega\ell}$, we can numerically solve the ODE (3.5) to high precision using the Mathematica (TM) function 'NDSolve' .

3.1.1 Boundary conditions for the up-modes

The up-modes take on the simple form $\phi^{\rm up}_{\omega\ell} \sim {\rm e}^{i\omega r^*}/r$ as $r \to \infty$, and they are illustrated on the left-hand side of Figure 1. To numerically obtain their value at a given suitably large radius, which we denote by $r_{\rm inf}$, we substitute the ansatz

$$\phi^{\rm up}_{\omega\ell} \sim \frac{{\rm e}^{i\omega r^*}}{r}\, {\rm e}^{v(r)}\,, \tag{3.6}$$

with

$$v(r) := \sum_{n=1}^{\infty} \frac{c_n}{r^n}\,, \tag{3.7}$$

into (3.5). This leads to an equation for $v(r)$:

$$r^2(r-2M)v''(r) + r^2(r-2M)(v'(r))^2 + 2r\left(M + i\omega r^2\right)v'(r) - (\ell(\ell+1)r + 2M) = 0\,. \tag{3.8}$$

We substitute (3.7) into (3.8) and collect inverse powers of r. The coefficient of each power of r must be set equal to zero. The lowest power leads to an equation only involving c_1, the next power only involves c_1 and c_2, the next only c_1, c_2 and c_3, and so on. Starting with c_1, we iteratively solve for the c_i by substituting the previous result into the next equation to be solved. In practice, the upper limit in the sum (3.7) is replaced by some suitable cut-off, denoted as $n_{\rm inf}$. This means that the highest power we can trust in the r^{-1} expansion of (3.8) is $r^{-(n_{\rm inf}-2)}$, and the highest coefficient obtained is $c_{n_{\rm inf}}$. The values of $n_{\rm inf}$ and $r_{\rm inf}$ are determined by the desired numerical accuracy.

The initial conditions for $\phi^{\rm up}_{\omega\ell}$ and $\phi^{\rm up\prime}_{\omega\ell}$ are computed using these c_i and by evaluating at $r_{\rm inf}$:

$$\begin{aligned}\phi^{\rm up}_{\omega\ell}(r_{\rm inf}) &= \frac{\mathrm{e}^{i\omega r^*(r_{\rm inf})}}{r_{\rm inf}}\,\mathrm{e}^{v(r_{\rm inf})}\,,\\ \phi^{\rm up\prime}_{\omega\ell}(r_{\rm inf}) &= \frac{d}{dr}\left[\frac{\mathrm{e}^{i\omega r^*(r)}}{r}\,\mathrm{e}^{v(r)}\right]_{r=r_{\rm inf}}\,.\end{aligned} \tag{3.9}$$

These initial conditions become more accurate as $r_{\rm inf}$ and $n_{\rm inf}$ increase.

We computed the initial conditions (3.9) in Mathematica (TM) for $n_{\rm inf} = 100$ and $r_{\rm inf} = 15000M$, where we set $M = 1$ in the code and re-inserted the appropriate factors of M in the computed physical answers by dimensional analysis. Having computed the boundary conditions, we then used Mathematica's 'NDSolve' function to generate our up-modes $\phi^{\rm up}_{\omega\ell}$ for a given (ω, ℓ). We sought a result for the transition rate that was accurate to around 3 or 4 decimal places. As we shall see later, the Wightman function is constructed using tens of thousands of points in (ω, ℓ) parameter space, and a high precision in the individual $\phi^{\rm up}_{\omega\ell}, \phi^{\rm in}_{\omega\ell}$ modes is essential. In order to get the desired accuracy results for the transition rate, we used the following precision settings in 'NDSolve'; we set 'WorkingPrecision' to around 40, 'AccuracyGoal' to around 32 and 'PrecisionGoal' to around 20. With these settings, the results for $\phi^{\rm up}_{\omega\ell}, \phi^{\rm in}_{\omega\ell}$ did not change to around 10 decimal places upon further increases to the 'NDSolve' precision settings.

3.1.2 Boundary conditions for the in-modes

The in-modes are the modes that take on a simple ingoing form at the horizon, $\mathrm{e}^{-i\omega r^*}/r$, but at any finite radius are a complicated superposition of

ingoing and outgoing plane waves because of the scattering from the gravitational potential. They are illustrated on the right-hand side of Figure 1. Thus, our strategy is to compute the initial conditions of the in-modes at the horizon, taking

$$\phi^{\rm in}_{\omega\ell} \sim \frac{{\rm e}^{-i\omega r^*}}{r} w(r) \tag{3.10}$$

as our ansatz, with

$$w(r) := \sum_{n=0}^{\infty} b_n \left(r-2M\right)^n \,, \tag{3.11}$$

and $b_0 = 1$.

We substitute (3.10) into (3.5) to obtain an equation in $w(r)$ that reads

$$r^2(r-2M)w''(r) + 2r\left(M - ir^2\omega\right)w'(r) - (\ell(\ell+1)r + 2M)w(r) = 0\,. \tag{3.12}$$

Using (3.11) in (3.12), a recursion relation can be obtained [31]:

$$\begin{aligned} &b_0 = 1\,, b_{-1} = b_{-2} = 0\,, \\ &b_n = -\frac{[-12i\omega M(n-1) + (2n-3)(n-1) - (\ell(\ell+1)+1)]}{2M\left(n^2 - i4Mn\omega\right)} b_{n-1} \\ &- \frac{[(n-2)(n-3) - i12M\omega(n-2) - \ell(\ell+1)]}{4M^2\left(n^2 - i4Mn\omega\right)} b_{n-2} \\ &+ \frac{i\omega(n-3)}{2M^2\left(n^2 - i4Mn\omega\right)} b_{n-3}\,. \end{aligned} \tag{3.13}$$

We are now in a position to compute the initial conditions for $\phi^{\rm in}_{\omega\ell}$ and $\phi^{\rm in}{}'_{\omega\ell}$. We use these b_i with the upper limit of the sum (3.11) replaced by some finite integer n_H, determined by the accuracy requirements, and we evaluate at the near horizon radius r_H, obtaining

$$\begin{aligned} \phi^{\rm in}_{\omega\ell}(r_H) &= \frac{{\rm e}^{-i\omega r^*(r_H)}}{r_H} w(r_H)\,, \\ \phi^{\rm in}{}'_{\omega\ell}(r_H) &= \frac{d}{dr}\left[\frac{{\rm e}^{-i\omega r^*(r)}}{r} w(r)\right]_{r=r_H}\,. \end{aligned} \tag{3.14}$$

In practice, the initial conditions (3.14) were computed in Mathematica (TM) for $n_H = 200$ and $r_H = (20,000,001/10,000,000)M$. Given these boundary conditions, we used Mathematica's 'NDSolve' function to generate our in-modes $\phi^{\rm in}_{\omega\ell}$ for a given (ω, ℓ), with the same precision settings as for the up-modes.

3.2 Normalisation

We choose a basis whose asymptotic behaviour as $r^* \to \pm\infty$ is

$$\tilde{\Phi}^{\rm in}_{\omega\ell}(r) \sim \begin{cases} B^{\rm in}_{\omega\ell}\, {\rm e}^{-i\omega r^*}, & r \to 2M\,, \\ r^{-1}\, {\rm e}^{-i\omega r^*} + A^{\rm in}_{\omega\ell} r^{-1}\, {\rm e}^{+i\omega r^*}, & r \to \infty\,, \end{cases} \tag{3.15}$$

and

$$\tilde{\Phi}^{\rm up}_{\omega\ell}(r) \sim \begin{cases} A^{\rm up}_{\omega\ell}\, {\rm e}^{-i\omega r^*} + {\rm e}^{+i\omega r^*}, & r \to 2M\,, \\ B^{\rm up}_{\omega\ell} r^{-1}\, {\rm e}^{+i\omega r^*}, & r \to \infty\,. \end{cases} \tag{3.16}$$

The reflection and transmission coefficients satisfy the following Wronskian relations:

$$\begin{aligned} B^{\rm up}_{\omega\ell} &= (2M)^2 B^{\rm in}_{\omega\ell}\,, \\ |A^{\rm in}_{\omega\ell}|^2 &= 1 - 4M^2 |B^{\rm in}_{\omega\ell}|^2\,, \\ |A^{\rm in}_{\omega\ell}|^2 &= |A^{\rm up}_{\omega\ell}|^2\,, \\ |A^{\rm up}_{\omega\ell}|^2 &= 1 - \frac{|B^{\rm up}_{\omega\ell}|^2}{4M^2}\,, \end{aligned} \tag{3.17}$$

and we can express the transmission and reflection coefficients by

$$\begin{aligned} B^{\rm up}_{\omega\ell} &= \frac{(2M) 2i\omega}{W[\rho^{\rm in}_{\omega\ell}, \rho^{\rm up}_{\omega\ell}]}\,, \\ A^{\rm up}_{\omega\ell} &= -\frac{W[\rho^{\rm in}_{\omega\ell}, \rho^{\rm up*}_{\omega\ell}]^*}{W[\rho^{\rm in}_{\omega\ell}, \rho^{\rm up}_{\omega\ell}]}\,, \\ A^{\rm in}_{\omega\ell} &= -\frac{W[\rho^{\rm in}_{\omega\ell}, \rho^{\rm up*}_{\omega\ell}]}{W[\rho^{\rm in}_{\omega\ell}, \rho^{\rm up}_{\omega\ell}]}\,, \end{aligned} \tag{3.18}$$

where $\rho^{\rm in}_{\omega\ell}$ and $\rho^{\rm up}_{\omega\ell}$ are the unnormalised modes associated with equations (3.3) and (3.5), which are the modes we solve for in the Mathematica (TM) code.

It is convenient to replace $\tilde{\Phi}^{\rm in}_{\omega\ell}$ and $\tilde{\Phi}^{\rm up}_{\omega\ell}$ with the un-tilded modes $\Phi^{\rm in}_{\omega\ell}$ and $\Phi^{\rm up}_{\omega\ell}$, defined by

$$\begin{aligned} \Phi^{\rm in}_{\omega\ell} &= \tilde{\Phi}^{\rm in}_{\omega\ell}\,, \\ \Phi^{\rm up}_{\omega\ell} &= \frac{\tilde{\Phi}^{\rm up}_{\omega\ell}}{2M}\,. \end{aligned} \tag{3.19}$$

Using the Wronskian relations (3.17), it can be verified that the functions $R_{\omega,\ell} := r\Phi_{\omega,\ell}$ are normalised as

$$\int_{-\infty}^{\infty} {\rm d}r^*\, R_{\omega_1,\ell}(r) R^*_{\omega_2,\ell}(r) = 2\pi\delta(\omega_1 - \omega_2)\,, \tag{3.20}$$

where we have suppressed the superscripts "in" and "up".

The normalised modes in this basis can be expressed in terms of the modes that we explicitly solve for in Mathematica (TM), $\phi^{\rm up}_{\omega\ell}$ and $\phi^{\rm in}_{\omega\ell}$, which were discussed in Section 3.1. The result is

$$\begin{aligned}\Phi^{\rm in}_{\omega\ell} &= \frac{B^{\rm up}_{\omega\ell}}{2M}\,\phi^{\rm in}_{\omega\ell}(r)\,,\\ \Phi^{\rm up}_{\omega\ell} &= \frac{B^{\rm up}_{\omega\ell}}{2M}\,\phi^{\rm up}_{\omega\ell}(r)\,.\end{aligned} \tag{3.21}$$

With this solution, we introduce the basis functions $u^{\rm in}_{\omega\ell m}$ and $u^{\rm up}_{\omega\ell m}$ by

$$\begin{aligned}u^{\rm in}_{\omega\ell m}(\mathsf{x}) &= \frac{1}{\sqrt{4\pi\omega}}\Phi^{\rm in}_{\omega\ell}(r)Y_{\ell m}(\theta,\phi)\,{\rm e}^{-i\omega t}\,,\\ u^{\rm up}_{\omega\ell m}(\mathsf{x}) &= \frac{1}{\sqrt{4\pi\omega}}\Phi^{\rm up}_{\omega\ell}(r)Y_{\ell m}(\theta,\phi)\,{\rm e}^{-i\omega t}\,,\end{aligned} \tag{3.22}$$

where $\omega > 0$. These modes are positive frequency with respect to the Schwarzschild time translation Killing vector ∂_t.

Using the Wronskian relations (3.17), it can be verified that these modes satisfy the orthonormality relations

$$\begin{aligned}(u^{\rm up}_{\omega\ell m}, u^{\rm up}_{\omega'\ell'm'}) &= \delta_{\ell\ell'}\delta_{mm'}\delta\left(\omega-\omega'\right)\,,\\ \left(u^{\rm in}_{\omega\ell m}, u^{\rm in}_{\omega'\ell'm'}\right) &= \delta_{\ell\ell'}\delta_{mm'}\delta\left(\omega-\omega'\right)\,,\\ \left(u^{\rm in}_{\omega\ell m}, u^{\rm up}_{\omega'\ell'm'}\right) &= 0\,,\end{aligned} \tag{3.23}$$

where the Klein-Gordon (indefinite) inner product on a spacelike hyperplane of simultaneity at instant t is defined by

$$(\phi,\chi) = -i\int_{2M}^{\infty}{\rm d}r\,\frac{r^2}{(1-2M/r)}\int_0^{\pi}{\rm d}\theta\,\sin\theta\int_0^{2\pi}{\rm d}\phi\,\left[\phi\partial_t\chi^* - (\partial_t\phi)\,\chi^*\right]\,. \tag{3.24}$$

The complex conjugate modes satisfy similar orthonormality relations with a minus sign, and the inner product relation between the modes (3.22) and the complex conjugates vanish.

4 Which quantum state?

We shall analyse the transition rate when the field is in the Hartle-Hawking state, the Boulware state and the Unruh state. In this section, we provide a brief reminder of the properties of each of the three states.

4.1 The Hartle-Hawking state

The Hartle-Hawking state is regular across the both the past and future horizon, and it reduces to a thermal heat bath at spatial infinity with temperature $T_H = \kappa/(2\pi)$, where the surface gravity, κ, is defined by $\kappa := 1/(4M)$.

In order to construct the Wightman function for the quantum field in the Hartle-Hawking state, we must expand the quantum field in terms of the modes that have the analytic properties of positive-frequency plane waves with respect to the horizon generators; these modes take the form [22, 32]

$$\begin{aligned}
w^{\rm in}_{\omega\ell m} &= \frac{1}{\sqrt{2\sinh\left(4\pi M\omega\right)}}\left(\mathrm{e}^{2\pi M\omega}\, u^{\rm in}_{\omega\ell m} + \mathrm{e}^{-2\pi M\omega}\, v^{\rm in*}_{\omega\ell m}\right) ,\\
\bar{w}^{\rm in}_{\omega\ell m} &= \frac{1}{\sqrt{2\sinh\left(4\pi M\omega\right)}}\left(\mathrm{e}^{-2\pi M\omega}\, u^{\rm in*}_{\omega\ell m} + \mathrm{e}^{2\pi M\omega}\, v^{\rm in}_{\omega\ell m}\right) ,\\
w^{\rm up}_{\omega\ell m} &= \frac{1}{\sqrt{2\sinh\left(4\pi M\omega\right)}}\left(\mathrm{e}^{2\pi M\omega}\, u^{\rm up}_{\omega\ell m} + \mathrm{e}^{-2\pi M\omega}\, v^{\rm up*}_{\omega\ell m}\right) ,\\
\bar{w}^{\rm up}_{\omega\ell m} &= \frac{1}{\sqrt{2\sinh\left(4\pi M\omega\right)}}\left(\mathrm{e}^{-2\pi M\omega}\, u^{\rm up*}_{\omega\ell m} + \mathrm{e}^{2\pi M\omega}\, v^{\rm up}_{\omega\ell m}\right) ,
\end{aligned} \tag{4.1}$$

where the v are functions analogous to u on the second exterior region of the Kruskal manifold. The modes are extended to the full Kruskal manifold by analytic continuation.

Expanding the quantum field ψ in terms of these modes gives

$$\psi = \sum_{\ell=0}^{\infty}\sum_{m=-\ell}^{+\ell}\int_0^\infty \mathrm{d}\omega\left(d^{\rm up}_{\omega\ell m} w^{\rm up}_{\omega\ell m} + \bar{d}^{\rm up}_{\omega\ell m}\bar{w}^{\rm up}_{\omega\ell m} + d^{\rm in}_{\omega\ell m} w^{\rm in}_{\omega\ell m} + \bar{d}^{\rm in}_{\omega\ell m}\bar{w}^{\rm in}_{\omega\ell m}\right) + \text{h.c.}\,. \tag{4.2}$$

The $d^{\rm a}$ and $\bar{d}^{\rm a}$ ($d^{\rm a\,\dagger}$ and $\bar{d}^{\rm a\,\dagger}$) operators, with ${\rm a}\in\{\rm in, up\}$, are the annihilation (creation) operators with respect to the w and $\bar{w}$ modes, and they satisfy

$$\begin{aligned}
\left[d^{\rm a}_{\omega\ell m}, d^{\rm a'\,\dagger}_{\omega'\ell'm'}\right] &= \delta\left(\omega-\omega'\right)\delta_{\rm aa'}\delta_{\ell\ell'}\delta_{mm'} ,\\
\left[\bar{d}^{\rm a}_{\omega\ell m}, \bar{d}^{\rm a'\,\dagger}_{\omega'\ell'm'}\right] &= \delta\left(\omega-\omega'\right)\delta_{\rm aa'}\delta_{\ell\ell'}\delta_{mm'}
\end{aligned} \tag{4.3}$$

with the commutators between barred and unbarred operators vanishing, and

$$d^{\rm a}_{\omega\ell m}|0_K\rangle = \bar{d}^{\rm a}_{\omega\ell m}|0_K\rangle = 0\,. \tag{4.4}$$

The state $|0_K\rangle$ is the Hartle-Hawking state, and it is normalised such that

$$\langle 0_K|0_K\rangle = 1\,. \tag{4.5}$$

In the exterior region of the hole, the modes (4.1) reduce to a simple form because the v functions vanish, and if we compute the Wightman function for the Hartle-Hawking state in the exterior region, we find

$$
\begin{aligned}
&W(\mathsf{x},\mathsf{x}') := \langle 0_K|\psi(\mathsf{x})\psi(\mathsf{x}')|0_K\rangle \\
&= \sum_{\ell=0}^{\infty}\sum_{m=-\ell}^{+\ell}\int_0^\infty \mathrm{d}\omega\,\frac{1}{8\pi\omega\sinh\left(4\pi M\omega\right)}\times \\
&\Bigg[\mathrm{e}^{4\pi M\omega - i\omega\Delta t}\,Y_{\ell m}(\theta,\phi)Y^*_{\ell m}(\theta',\phi')\left(\Phi^{\mathrm{up}}_{\omega\ell}(r)\,\Phi^{\mathrm{up}*}_{\omega\ell}(r') + \Phi^{\mathrm{in}}_{\omega\ell}(r)\,\Phi^{\mathrm{in}\,*}_{\omega\ell}(r')\right) \\
&+ \mathrm{e}^{-4\pi M\omega + i\omega\Delta t}\,Y^*_{\ell m}(\theta,\phi)Y_{\ell m}(\theta',\phi')\left(\Phi^{\mathrm{up}*}_{\omega\ell}(r)\,\Phi^{\mathrm{up}}_{\omega\ell}(r') + \Phi^{\mathrm{in}\,*}_{\omega\ell}(r)\,\Phi^{\mathrm{in}}_{\omega\ell}(r')\right)\Bigg],
\end{aligned}
\tag{4.6}
$$

with $\Delta t := t - t'$.

4.2 The Boulware state

The Boulware state is analogous to the Rindler state in Rindler spacetime, and it is not regular across the black hole horizon. The Boulware state reduces to the Minkowski vacuum at spatial infinity. To construct the Wightman function for the Boulware state, the quantum scalar field is expanded in terms of the modes (3.22), i.e.

$$
\psi = \sum_{\ell=0}^{\infty}\sum_{m=-\ell}^{+\ell}\int_0^\infty \mathrm{d}\omega\left(b^{\mathrm{up}}_{\omega\ell m}u^{\mathrm{up}}_{\omega\ell m} + b^{\mathrm{in}}_{\omega\ell m}u^{\mathrm{in}}_{\omega\ell m}\right) + \mathrm{h.c.}\,, \tag{4.7}
$$

where the b and $b^\dagger$ operators are respectively the annihilation and creation operators for the u modes that satisfy the commutation relations

$$
\left[b^{\mathrm{a}}_{\omega\ell m}, b^{\mathrm{a}'\,\dagger}_{\omega'\ell'm'}\right] = \delta\left(\omega-\omega'\right)\delta_{\mathrm{aa}'}\delta_{\ell\ell'}\delta_{mm'} \tag{4.8}
$$

with $\mathrm{a}\in\{\mathrm{in},\mathrm{up}\}$. The Boulware state $|0_B\rangle$ is defined by

$$
b^{\mathrm{a}}_{\omega\ell m}|0_B\rangle = 0 \tag{4.9}
$$

and normalised such that

$$
\langle 0_B|0_B\rangle = 1\,. \tag{4.10}
$$

Hence, in the exterior region, the Wightman function of a scalar field in the Boulware state can be expressed as

$$W(\mathsf{x},\mathsf{x}') := \langle 0_B|\psi(\mathsf{x})\psi(\mathsf{x}')|0_B\rangle$$
$$= \sum_{\ell=0}^{\infty}\sum_{m=-\ell}^{+\ell}\int_0^\infty \mathrm{d}\omega\,\frac{Y_{\ell m}(\theta,\phi)Y^*_{\ell m}(\theta',\phi')}{4\pi\omega}\,\mathrm{e}^{-i\omega\Delta t}$$
$$\times\left(\Phi^{\rm up}_{\omega\ell}(r)\,\Phi^{\rm up*}_{\omega\ell}(r') + \Phi^{\rm in}_{\omega\ell}(r)\,\Phi^{\rm in\,*}_{\omega\ell}(r')\right)\,. \quad (4.11)$$

4.3 The Unruh state

The Unruh state mimics the geometric effects of a collapsing star, and it represents a time-asymmetric flux of radiation from the black hole. The Unruh mode construction (4.1) is applied only to the up-modes that originate on $\mathscr{H}^-$ and not to the in-modes originating on $\mathscr{I}^-$. Hence, the Wightman function in the Unruh state is defined by first expanding the quantum scalar field as

$$\psi = \sum_{\ell=0}^{\infty}\sum_{m=-\ell}^{+\ell}\int_0^\infty \mathrm{d}\omega\left(d^{\rm up}_{\omega\ell m}w^{\rm up}_{\omega\ell m} + \bar{d}^{\rm up}_{\omega\ell m}\bar{w}^{\rm up}_{\omega\ell m} + b^{\rm in}_{\omega\ell m}u^{\rm in}_{\omega\ell m}\right) + \text{h.c.}\,, \quad (4.12)$$

where now

$$b^{\rm in}_{\omega\ell m}|0_U\rangle = d^{\rm up}_{\omega\ell m}|0_U\rangle = \bar{d}^{\rm up}_{\omega\ell m}|0_U\rangle = 0\,, \quad (4.13)$$

with $|0_U\rangle$ the Unruh state. The annihilation and creation operators b, d and $b^\dagger$, $d^\dagger$ satisfy the commutation relations given in (4.3) and (4.8).

Hence, the Wightman function of a scalar field in this state can be expressed as

$$W(\mathsf{x},\mathsf{x}') := \langle 0_U|\psi(\mathsf{x})\psi(\mathsf{x}')|0_U\rangle$$
$$= \sum_{\ell=0}^{\infty}\sum_{m=-\ell}^{+\ell}\int_0^\infty \mathrm{d}\omega\,\left[w^{\rm up}_{\omega\ell m}(\mathsf{x})w^{\rm up*}_{\omega\ell m}(\mathsf{x}') + \bar{w}^{\rm up}_{\omega\ell m}(\mathsf{x})\bar{w}^{\rm up*}_{\omega\ell m}(\mathsf{x}') + u^{\rm in}_{\omega\ell m}(\mathsf{x})u^{\rm in*}_{\omega\ell m}(\mathsf{x}')\right]\,. \quad (4.14)$$

In the exterior region, this reduces to

$$W(\mathsf{x},\mathsf{x}') = \sum_{\ell=0}^{\infty}\sum_{m=-\ell}^{+\ell}\int_0^\infty \mathrm{d}\omega \left[\frac{\mathrm{e}^{4\pi M\omega - i\omega\Delta t}\, Y_{\ell m}(\theta,\phi)Y^*_{\ell m}(\theta',\phi')\, \Phi^{\mathrm{up}}_{\omega\ell}(r)\, \Phi^{\mathrm{up}*}_{\omega\ell}(r')}{8\pi\omega\sinh(4\pi M\omega)}\right.$$
$$+ \frac{\mathrm{e}^{-4\pi M\omega + i\omega\Delta t}\, Y^*_{\ell m}(\theta,\phi)Y_{\ell m}(\theta',\phi')\, \Phi^{\mathrm{up}*}_{\omega\ell}(r)\, \Phi^{\mathrm{up}}_{\omega\ell}(r')}{8\pi\omega\sinh(4\pi M\omega)}$$
$$\left. + \frac{\mathrm{e}^{-i\omega\Delta t}\, Y_{\ell m}(\theta,\phi)Y^*_{\ell m}(\theta',\phi')\, \Phi^{\mathrm{in}}_{\omega\ell}(r)\, \Phi^{\mathrm{in}\,*}_{\omega\ell}(r')}{4\pi\omega}\right], \tag{4.15}$$

with $\Delta t := t - t'$.

5 Static detector

In this section, we specialise to a static detector: $r = r' = R$, $\Delta t = \Delta\tau/\sqrt{1-2M/R}$, and we can take $\theta = \theta' = \phi = \phi' = 0$ without loss of generality.

5.1 Hartle-Hawking state

When the detector is static, the Wightman function of the Hartle-Hawking state in the exterior region (4.6) reduces to the form

$$W(\mathsf{x},\mathsf{x}') = \sum_{\ell}\int_0^\infty \mathrm{d}\omega\, \frac{(2\ell+1)}{16\pi^2\omega\sinh(4\pi M\omega)}\left(|\,\Phi^{\mathrm{up}}_{\omega\ell}(R)|^2 + |\,\Phi^{\mathrm{in}}_{\omega\ell}(R)|^2\right)$$
$$\times\cosh\left[4\pi M\omega - \frac{i\omega\Delta\tau}{\sqrt{1-2M/R}}\right], \tag{5.1}$$

where we have used (14.30.4) from [33] to collapse the m-sum.

We now substitute (5.1) into the expression for the transition rate (2.4). After interchanging the order of the s- and ω-integrals and taking the regulator to zero, we arrive at

$$\dot{\mathcal{F}}(E) = \int_0^\infty \mathrm{d}\omega \sum_{l=0}^{\infty}\frac{(2\ell+1)}{16\pi^2\omega\sinh(4\pi M\omega)}\left(|\,\Phi^{\mathrm{up}}_{\omega\ell}(R)|^2 + |\,\Phi^{\mathrm{in}}_{\omega\ell}(R)|^2\right)$$
$$\times\int_{-\infty}^{\infty}\mathrm{d}s\;\mathrm{e}^{-iEs}\cosh\left[4\pi M\omega - \frac{i\omega s}{\sqrt{1-2M/R}}\right]. \tag{5.2}$$

The s-integral can be computed analytically, resulting in

$$\dot{\mathcal{F}}(E) = \int_0^\infty \mathrm{d}\omega \sum_{l=0}^{\infty} \frac{(2\ell+1)}{16\pi\omega \sinh(4\pi M\omega)} \left(|\,\Phi^{\mathrm{up}}_{\omega\ell}(R)|^2 + |\,\Phi^{\mathrm{in}}_{\omega\ell}(R)|^2 \right) \times \left[\mathrm{e}^{4\pi M\omega}\, \delta\left(E + \frac{\omega}{\sqrt{1-2M/R}} \right) + \mathrm{e}^{-4\pi M\omega}\, \delta\left(E - \frac{\omega}{\sqrt{1-2M/R}} \right) \right]. \tag{5.3}$$

The factors $|\,\Phi^{\mathrm{up}}_{\omega\ell}(R)|$ and $|\,\Phi^{\mathrm{in}}_{\omega\ell}(R)|$ can be extended to negative values of ω by symmetry. This allows one to write the transition rate as

$$\dot{\mathcal{F}}(E) = \sum_{l=0}^{\infty} \frac{(2\ell+1)}{4\pi} \sqrt{1-2M/R} \left(|\Phi^{\mathrm{up}}_{\tilde{\omega}\ell}(R)|^2 + |\Phi^{\mathrm{in}}_{\tilde{\omega}\ell}(R)|^2 \right) \times \left[\frac{\mathrm{e}^{-4\pi ME\sqrt{1-2M/R}}\, \Theta(-E)}{-4E\sqrt{1-2M/R} \sinh\left(-4\pi ME\sqrt{1-2M/R}\right)} + \frac{\mathrm{e}^{-4\pi ME\sqrt{1-2M/R}}\, \Theta(E)}{4E\sqrt{1-2M/R} \sinh\left(4\pi ME\sqrt{1-2M/R}\right)} \right], \tag{5.4}$$

where $\tilde{\omega} := E\sqrt{1-2M/R}$. This can further be simplified to

$$\dot{\mathcal{F}}(E) = \frac{1}{8\pi E} \frac{1}{\mathrm{e}^{E/T_{\mathrm{loc}}} - 1} \sum_{l=0}^{\infty} (2\ell+1) \left(|\Phi^{\mathrm{up}}_{\tilde{\omega}\ell}(R)|^2 + |\Phi^{\mathrm{in}}_{\tilde{\omega}\ell}(R)|^2 \right), \tag{5.5}$$

where T_{loc} is the local Hawking temperature, given by

$$T_{\mathrm{loc}} := \frac{1}{8\pi M\sqrt{1-2M/R}}. \tag{5.6}$$

The non-Planckian factor in (5.5) can be thought of as the local density of states [27]. This result can be compared to the asymptotic form found in [34], but here we are most interested in performing the calculation in the interesting region near the black hole.

The result (5.5) manifestly obeys the KMS condition by virtue of the fact that the modes $\Phi^{\mathrm{up}}_{\tilde{\omega}\ell}$ and $\Phi^{\mathrm{in}}_{\tilde{\omega}\ell}$ only depend on the absolute value of $\tilde{\omega} := E\sqrt{1-2M/R}$; hence, the modes only depend on the absolute value of excitation energy. Thus, the condition

$$\dot{\mathcal{F}}(E) = \mathrm{e}^{-E/T_{\mathrm{loc}}}\, \dot{\mathcal{F}}(-E) \tag{5.7}$$

is obeyed, and the transition rate is thermal in the temperature T_{loc}. Our mode sum treatment, hence, reproduces the thermality result that was deduced in [8] from the complex analytic properties of the Wightman function.

5.2 Boulware state

For the static detector and the field in the Boulware state, the Wightman function (4.11) reduces to

$$W(\mathsf{x},\mathsf{x}') = \sum_{\ell=0}^{\infty} \int_0^{\infty} \mathrm{d}\omega \, \frac{(2\ell+1)}{16\pi^2\omega} \, \mathrm{e}^{-i\omega\Delta\tau/\sqrt{1-2M/R}} \left(|\, \Phi^{\mathrm{up}}_{\omega\ell}(R)|^2 + |\, \Phi^{\mathrm{in}}_{\omega\ell}(R)|^2 \right) \,, \tag{5.8}$$

where again (14.30.4) in [33] has been used.

We substitute the Wightman function (5.8) into transition rate (2.4) and commute the s- and ω-integrals to obtain

$$\begin{aligned} \dot{\mathcal{F}}\,(E) = \int_0^{\infty} \mathrm{d}\omega \, \sum_{l=0}^{\infty} \frac{(2\ell+1)}{16\pi^2\omega} \left(|\, \Phi^{\mathrm{up}}_{\omega\ell}(R)|^2 + |\, \Phi^{\mathrm{in}}_{\omega\ell}(R)|^2 \right) \\ \times \int_{-\infty}^{\infty} \mathrm{d}s \; \mathrm{e}^{-iEs} \, \mathrm{e}^{-i\omega s/\sqrt{1-2M/R}} \,, \end{aligned} \tag{5.9}$$

and performing the s-integral gives

$$\begin{aligned} \dot{\mathcal{F}}\,(E) = \int_0^{\infty} \mathrm{d}\omega \, \sum_{l=0}^{\infty} \frac{(2\ell+1)}{8\pi\omega} \left(|\, \Phi^{\mathrm{up}}_{\omega\ell}(R)|^2 + |\, \Phi^{\mathrm{in}}_{\omega\ell}(R)|^2 \right) \\ \times \delta\left(E + \frac{\omega}{\sqrt{1-2M/R}} \right) \,, \end{aligned} \tag{5.10}$$

which can be simplified to

$$\dot{\mathcal{F}}\,(E) = \frac{\Theta(-E)}{8\pi|E|} \sum_{l=0}^{\infty} (2\ell+1) \left(|\Phi^{\mathrm{up}}_{\tilde{\omega}\ell}(R)|^2 + |\Phi^{\mathrm{in}}_{\tilde{\omega}\ell}(R)|^2 \right) \,, \tag{5.11}$$

where $\tilde{\omega} := E\sqrt{1-2M/R}$.

We note that when the field is in the Boulware state, the transition rate for the static detector is only non-zero for negative energies of the detector, i.e. de-excitations. The result (5.11) is very similar to the transition rate for the inertial detector in flat spacetime, $-E\Theta(-E)/2\pi$, only with modifications due to the curvature of spacetime. This is what one would expect for the Boulware state.

5.3 Unruh state

For the static detector and the field in the Unruh state, the Wightman function (4.15) reduces to

$$W(\mathsf{x},\mathsf{x}') = \sum_{\ell=0}^{\infty} \int_0^{\infty} \mathrm{d}\omega \, \frac{(2\ell+1)}{16\pi^2\omega} \times \\ \left[\frac{|\,\Phi^{\mathrm{up}}_{\omega\ell}(R)|^2}{2\sinh(4\pi M\omega)} \left(\mathrm{e}^{4\pi\omega - i\omega\Delta\tau/\sqrt{1-2M/R}} + \mathrm{e}^{-4\pi\omega + i\omega\Delta\tau/\sqrt{1-2M/R}} \right) \right. \\ \left. + |\,\Phi^{\mathrm{in}}_{\omega\ell}(R)|^2 \, \mathrm{e}^{-i\omega\Delta\tau/\sqrt{1-2M/R}} \right], \tag{5.12}$$

where again (14.30.4) in [33] has been used.

We substitute the Wightman function (5.12) into transition rate (2.4), and after commuting the ω- and s-integrals, we can compute the s-integrals analytically, as in the Hartle-Hawking and Boulware states static calculations. The result for the transition rate is

$$\dot{\mathcal{F}}(E) = \sum_{l=0}^{\infty} \frac{(2\ell+1)}{4\pi} \left[\frac{|\Phi^{\mathrm{up}}_{\tilde{\omega}\ell}(R)|^2}{2E\,(\mathrm{e}^{E/T_{\mathrm{loc}}}-1)} - \frac{|\Phi^{\mathrm{in}}_{\tilde{\omega}\ell}(R)|^2}{2E}\Theta(-E) \right], \tag{5.13}$$

where $\tilde{\omega} := E\sqrt{1-2M/R}$ and T_{loc} is given by (5.6).

6 Circular-geodesic detector

In this section, we investigate the transition rate of a detector orbiting the Schwarzschild black hole on a circular geodesic. Explicitly, the detector trajectory is

$$r = R\,, \quad \theta = \pi/2\,, \quad t = a\tau\,, \quad \phi = a\Omega\tau\,, \tag{6.1}$$

where $R > 3M$ and

$$a := \sqrt{R/(R-3M)}\,, \\ \Omega := \frac{d\phi}{dt} = \sqrt{M/R^3}\,. \tag{6.2}$$

Trajectories with $3M < R \leq 6M$ are unstable, and trajectories with $R > 6M$ are stable.

6.1 Hartle-Hawking state

We first obtain the Wightman function for a detector on a circular geodesic in the Hartle-Hawking state by substituting (6.1) into (4.6) and expanding the spherical harmonics. We obtain

$$W(\mathsf{x},\mathsf{x}') = \sum_{\ell=0}^{\infty}\sum_{m=-\ell}^{+\ell}\int_0^\infty \mathrm{d}\omega\, \frac{(\ell-m)!(2\ell+1)|P_\ell^m(0)|^2}{32\pi^2\omega(l+m)!\sinh(4\pi M\omega)}\times \\ \left(|\,\Phi^{\rm up}_{\omega\ell}(R)|^2+|\,\Phi^{\rm in}_{\omega\ell}(R)|^2\right)\left[\mathrm{e}^{4\pi M\omega-ia\omega s+ima\Omega s}+\mathrm{e}^{-4\pi M\omega+ia\omega s-ima\Omega s}\right]. \tag{6.3}$$

Additionally, one can use (14.30.5) of [33] to see that the contribution to the Wightman function will vanish unless $\ell+m$ is even. This means that for a given ℓ we can set $m\equiv\ell\,(\mathrm{mod}2)$.

We use (6.3) in (2.4), and as in the static section, we can evaluate the s-integral analytically. The resulting expression reads

$$\dot{\mathcal{F}}(E) = \sum_{\ell=0}^{\infty}\sum_{m=-\ell}^{\ell}\int_0^\infty \mathrm{d}\omega\, \frac{(\ell-m)!(2\ell+1)|P_\ell^m(0)|^2}{16\pi\omega(l+m)!\sinh(4\pi M\omega)}\left(|\,\Phi^{\rm up}_{\omega\ell}(R)|^2+|\,\Phi^{\rm in}_{\omega\ell}(R)|^2\right) \\ \times\left[\mathrm{e}^{4\pi M\omega}\,\delta\left(E+a\omega-ma\Omega\right)+\mathrm{e}^{-4\pi M\omega}\,\delta\left(E-a\omega+ma\Omega\right)\right]. \tag{6.4}$$

Evaluating the integral over ω, we finally obtain

$$\dot{\mathcal{F}}(E) = \sum_{\ell=0}^{\infty}\sum_{m=-\ell}^{+\ell}\frac{(\ell-m)!(2\ell+1)|P_\ell^m(0)|^2}{16\pi(l+m)!}\times \\ \left[\frac{\left(|\Phi^{\rm up}_{\omega_-\ell}(R)|^2+|\Phi^{\rm in}_{\omega_-\ell}(R)|^2\right)\mathrm{e}^{4\pi M\omega_-}}{a\omega_-\sinh(4\pi M\omega_-)}\Theta(ma\Omega-E)\right. \\ \left.+\frac{\left(|\Phi^{\rm up}_{\omega_+\ell}(R)|^2+|\Phi^{\rm in}_{\omega_+\ell}(R)|^2\right)\mathrm{e}^{-4\pi M\omega_-}}{a\omega_+\sinh(4\pi M\omega_+)}\Theta(ma\Omega+E)\right], \tag{6.5}$$

with

$$\omega_\pm := (ma\Omega\pm E)/a\,. \tag{6.6}$$

6.2 Boulware state

We start by substituting (6.1) into (4.11), and we expand the spherical harmonics. The Wightman function then reads

$$W(\mathsf{x},\mathsf{x}') = \sum_{\ell=0}^{\infty}\sum_{m=-\ell}^{\ell}\int_0^\infty \mathrm{d}\omega\, \frac{(\ell-m)!(2\ell+1)|P_\ell^m(0)|^2}{16\pi^2\omega(\ell+m)!}\,\mathrm{e}^{ima\Omega\Delta\tau-ia\omega\Delta\tau} \\ \times\left(|\,\Phi^{\rm up}_{\omega\ell}(R)|^2+|\,\Phi^{\rm in}_{\omega\ell}(R)|^2\right). \tag{6.7}$$

We substitute this Wightman function into (2.4), and we evaluate the s-integral analytically. The resulting expression for the transition rate is

$$\dot{\mathcal{F}}(E) = \sum_{\ell=0}^{\infty} \sum_{m=-\ell}^{\ell} \int_0^{\infty} \mathrm{d}\omega \, \frac{(\ell-m)!(2\ell+1)|P_\ell^m(0)|^2}{8\pi\omega(\ell+m)!} \left(|\,\Phi^{\mathrm{up}}_{\omega\ell}(R)|^2 + |\,\Phi^{\mathrm{in}}_{\omega\ell}(R)|^2 \right) \times \delta\left(a\omega - (ma\Omega - E)\right) . \tag{6.8}$$

Evaluating the ω-integral yields

$$\dot{\mathcal{F}}(E) = \frac{1}{a} \sum_{\ell=0}^{\infty} \sum_{m=-\ell}^{\ell} \frac{(\ell-m)!(2\ell+1)|P_\ell^m(0)|^2}{8\pi\omega_-(\ell+m)!} \left(|\Phi^{\mathrm{up}}_{\omega_-\ell}(R)|^2 + |\Phi^{\mathrm{in}}_{\omega_-\ell}(R)|^2 \right) \times \Theta\left(ma\Omega - E\right) , \tag{6.9}$$

with

$$\omega_- := (ma\Omega - E)/a \, . \tag{6.10}$$

6.3 Unruh state

This time we substitute (6.1) into (4.15), and we expand the spherical harmonics. The Wightman function then reads

$$W(\mathsf{x},\mathsf{x}') = \sum_{\ell=0}^{\infty} \sum_{m=-\ell}^{\ell} \int_0^{\infty} \mathrm{d}\omega \, \frac{(\ell-m)!(2\ell+1)|P_\ell^m(0)|^2}{16\pi^2(\ell+m)!} \times \left[\frac{|\,\Phi^{\mathrm{up}}_{\omega\ell}(R)|^2 \left(\mathrm{e}^{4\pi M\omega - ia\omega\Delta\tau + ima\Omega\Delta\tau} + \mathrm{e}^{-4\pi M\omega + ia\omega\Delta\tau - ima\Omega\Delta\tau} \right)}{2\omega \sinh\left(4\pi M\omega\right)} + \frac{|\,\Phi^{\mathrm{in}}_{\omega\ell}(R)|^2 \, \mathrm{e}^{-ia\omega\Delta\tau + ima\Omega\Delta\tau}}{\omega} \right] . \tag{6.11}$$

Substituting this Wightman function into (2.4) and evaluating the s-integral analytically, the transition rate is

$$\dot{\mathcal{F}}(E) = \sum_{\ell=0}^{\infty} \sum_{m=-\ell}^{\ell} \int_0^{\infty} \mathrm{d}\omega \, \frac{(\ell-m)!(2\ell+1)|P_\ell^m(0)|^2}{8\pi(\ell+m)!} \times \left[\frac{|\,\Phi^{\mathrm{up}}_{\omega\ell}(R)|^2}{2\omega \sinh\left(4\pi M\omega\right)} \left(\mathrm{e}^{4\pi M\omega} \, \delta\left(E + a\omega - ma\Omega\right) + \mathrm{e}^{-4\pi M\omega} \, \delta\left(E - a\omega + ma\Omega\right) \right) + \frac{|\,\Phi^{\mathrm{in}}_{\omega\ell}(R)|^2}{\omega} \delta\left(E + a\omega - ma\Omega\right) \right] . \tag{6.12}$$

Evaluating the ω-integral yields

$$\dot{\mathcal{F}}(E) = \frac{1}{a}\sum_{\ell=0}^{\infty}\sum_{m=-\ell}^{\ell}\frac{(\ell-m)!(2\ell+1)|P_\ell^m(0)|^2}{8\pi(\ell+m)!}\times$$
$$\left[\left(\frac{|\Phi^{\rm up}_{\omega_-\ell}(R)|^2}{2\omega_-\sinh(4\pi M\omega_-)}\,{\rm e}^{4\pi M\omega_-}+\frac{|\Phi^{\rm in}_{\omega_-\ell}(R)|^2}{\omega_-}\right)\Theta(ma\Omega-E)\right.$$
$$\left.+\,\frac{|\Phi^{\rm up}_{\omega_+\ell}(R)|^2}{2\omega_+\sinh(4\pi M\omega_+)}\,{\rm e}^{-4\pi M\omega_+}\,\Theta(ma\Omega+E)\right], \quad (6.13)$$

with

$$\omega_\pm := (ma\Omega \pm E)/a\,. \quad (6.14)$$

6.4 Evaluation

It proves only necessary to compute $\Phi^{\rm up}_{\omega_\pm,\ell}, \Phi^{\rm in}_{\omega_\pm,\ell}$, where $\omega_\pm := (ma\Omega \pm E)/a$, over the positive range $E > 0,\ m \geq 0$ in order to have all the data we need to reconstruct the full transition rate over both negative and positive E and m. The reason for this is the fact that the absolute square of the modes only depends on the absolute value of ω, and $\omega_\pm(m,E)$ can always be related to $\pm\omega_\pm(|m|,|E|)$. For example, assuming we wished to compute the $|\Phi^{\rm up}_{\omega_+,\ell}|^2, |\Phi^{\rm in}_{\omega_+,\ell}|^2$ for a term in the sum where both $E, m < 0$, we can observe that

$$\begin{aligned}\omega_+(-|m|,-|E|) &= \frac{-|m|a\Omega-|E|}{a}\\ &= -\frac{|m|a\Omega+|E|}{a}\\ &= -\omega_+(|m|,|E|)\,.\end{aligned} \quad (6.15)$$

Thus, if we have already computed the modes at $\omega_+(|m|,|E|)$, then by the fact that $|\omega_+(-|m|,-|E|)| = |\omega_+(|m|,|E|)|$ and the independence of $|\Phi^{\rm up}_{\omega_+,\ell}|^2, |\Phi^{\rm in}_{\omega_+,\ell}|^2$ on the overall sign of ω, we see that we also have the value of the absolute value squared of the modes over the range where both $E,\ m < 0$. Further relations are

$$\begin{aligned}\omega_+(-|m|,|E|) &= -\omega_-(|m|,|E|)\,,\\ \omega_+(|m|,-|E|) &= \omega_-(|m|,|E|)\,,\\ \omega_-(-|m|,-|E|) &= -\omega_-(|m|,|E|)\,,\\ \omega_-(-|m|,|E|) &= -\omega_+(|m|,|E|)\,,\\ \omega_-(|m|,-|E|) &= \omega_+(|m|,|E|)\,.\end{aligned} \quad (6.16)$$

7 Comparison with a Rindler observer

The analogy between the right-hand Rindler wedge and the exterior Schwarzschild spacetime is well known [22]. It seems a natural question to ask whether the experience of the static detector when the field is in the Hartle-Hawking state, which we have described in the previous sections, is related to the experience of a detector in Rindler spacetime on a Rindler trajectory with the field in the Minkowski vacuum. Similarly, we ask if the experience of a detector on a circular geodesic in Schwarzschild spacetime is related to that of a detector on a Rindler trajectory but given some boost in the transverse direction [35].

7.1 Static detector comparison with Rindler detector

The Rindler observer's trajectory in (3+1)-dimensional Minkowski spacetime is

$$\mathsf{x}(\tau) = \frac{1}{a}\big(\sinh(a\tau), \cosh(a\tau), L, 0\big)\,, \tag{7.1}$$

where the positive constant a is the proper acceleration, τ is the proper time, and we have introduced the real-valued constant L for later convenience. With the quantum field in the Minkowski vacuum, the transition rate for a detector on the Rindler trajectory is [22]

$$\dot{\mathcal{F}}(E) = \frac{E}{2\pi\big(\mathrm{e}^{2\pi E/a} - 1\big)}\,, \tag{7.2}$$

which is thermal at the temperature $a/(2\pi)$. We choose to compare the Rindler response to the Schwarzschild response by matching the trajectories so that the Rindler temperature $a/(2\pi)$ is equal to the local Hawking temperature T_{loc} (5.6). This gives

$$a = 1/\big(4M\sqrt{1 - 2M/R}\,\big)\,. \tag{7.3}$$

We note that the proper acceleration of a static worldline in Schwarzschild is given by

$$a_S = M/\big(R^2\sqrt{1 - 2M/R}\,\big)\,. \tag{7.4}$$

From (7.3) and (7.4) we hence see that matching the local temperatures is not the same as matching the proper accelerations, although the two become asymptotically equal in the near-horizon limit, where the analogy between the Rindler and Schwarzschild spacetimes is the closest: as $R \to 2M$, we have $a \to \infty$ and $a_S \to \infty$ so that $a/a_S \to 1$ and $a - a_S \to 0$.

7.2 Circular-geodesic detector compared with Rindler plus transverse drift detector

Next, consider the Rindler observer but with constant drift-velocity in the transverse y-direction:

$$\mathsf{x}(\tau')_{\rm drift} = \frac{1}{a}\big(\sinh(q\tau'), \cosh(q\tau'), p\tau', 0\big)\,, \tag{7.5}$$

where a, q and p are positive constants and τ' is the proper time. In order for the four-velocity to be correctly normalised, we require that

$$a^2 = q^2 - p^2\,. \tag{7.6}$$

If we take $p \to 0$, this trajectory becomes the Rindler trajectory with proper acceleration a.

In Schwarzschild spacetime, the static detector has four-velocity given by

$$\mathsf{U}_{\rm static} = \left(\sqrt{\frac{R}{R-2M}}, 0, 0, 0\right)\,, \tag{7.7}$$

and the circular-geodesic trajectory, specified by (6.1) and (6.2), has four-velocity

$$\mathsf{U}_{\rm circ} = \left(\sqrt{\frac{R}{R-3M}}, 0, 0, \sqrt{\frac{M}{R^2(R-3M)}}\right)\,. \tag{7.8}$$

It follows that

$$\mathsf{U}_{\rm circ}\cdot\mathsf{U}_{\rm static} = -\sqrt{\frac{R-2M}{R-3M}}\,. \tag{7.9}$$

We choose to compare the Rindler detector with transverse drift (RDTD) to the circular-geodesic Schwarzschild detector by matching the drift velocity in Rindler to the orbital velocity in Schwarzschild. In terms of the four-velocity vectors, this amounts to setting $\mathsf{U}_{\rm RDTD}\cdot\mathsf{U}_{\rm Rind} = \mathsf{U}_{\rm circ}\cdot\mathsf{U}_{\rm static}$, where $\mathsf{U}_{\rm Rind}$ and $\mathsf{U}_{\rm RDTD}$ are the four-velocity of the Rindler detector and RDTD respectively. As the circular geodesics exist only for $R > 3M$, we note that this comparison cannot be extended to the near-horizon limit, where the analogy between the Rindler and Schwarzschild spacetime is the closest.

To implement the matching, the dot product in $\mathsf{U}_{\rm RDTD}\cdot\mathsf{U}_{\rm Rind}$ must be evaluated when the Rindler and RDTD observers are at the same spacetime point. Comparison of (7.1) and (7.5) shows that in order to be at the same point we must take $a\tau = q\tau'$ and $\tau' = L/p$. This means that at this spacetime point

$$\begin{aligned}\mathsf{U}_{\rm Rind} &= \big(\cosh(qL/p), \sinh(qL/p), 0, 0\big)\,,\\ \mathsf{U}_{\rm RDTD} &= \Big(\frac{q}{a}\cosh(qL/p), \frac{q}{a}\sinh(qL/p), \frac{p}{a}, 0\Big)\,,\end{aligned} \tag{7.10}$$

so that

$$\mathsf{U}_{\text{Rind}} \cdot \mathsf{U}_{\text{RDTD}} = -\frac{q}{a}\,. \tag{7.11}$$

We want

$$q = \frac{1}{4M}\sqrt{\frac{R}{R-3M}}\,, \tag{7.12}$$

and by virtue of (7.3) and (7.6), we have

$$p = \frac{1}{4M}\sqrt{\frac{MR}{(R-3M)(R-2M)}}\,. \tag{7.13}$$

The transition rate for the RDTD can now easily be computed. By (7.5), we first note that the Minkowski interval is

$$\Delta\mathsf{x}^2 = \frac{p^2}{a^2}\Delta\tau^2 - \frac{4}{a^2}\sinh^2\left(\frac{q\Delta\tau}{2}\right). \tag{7.14}$$

This can be substituted into the transition rate found in [12]. The comparison will be examined in Section 8.

We also would like to see if the comparison between the detector on a circular geodesic in Schwarzschild and the RDTD becomes better if we make the transverse direction, in which the Rindler detector is drifting, periodic. The proper-time period for the circular-geodesic detector in Schwarzschild to complete a loop is

$$P := 2\pi\sqrt{R^2(R-3M)/M}\,. \tag{7.15}$$

We wish to identify the transverse direction of Minkowski spacetime that our RDTD exists on by the same period in proper time. This means identifying the points

$$\begin{aligned} y(\tau) &\sim y(\tau + nP) \\ &= y(\tau) + npP/a\,, \end{aligned} \tag{7.16}$$

where n is an integer and y is the transverse direction in which the drift occurs. In order to get the transition rate of the RDTD on flat spacetime with periodic boundary conditions in the transverse drift direction, we employ the method of images. This results in the square interval

$$\Delta\mathsf{x}_n^2 = -\frac{4}{a^2}\sinh^2\left(\frac{q\Delta\tau}{2}\right) + \left(\frac{p\Delta\tau}{a} + \frac{npP}{a}\right)^2, \quad n \in \mathbb{Z}\,. \tag{7.17}$$

We substitute this interval into the transition rate (2.4). Because the periodicity could lead to singularities at $\Delta\tau \neq 0$, not dealt with by the Hadamard short distance form, we need the form of the transition rate with regulator

intact. The exception, of course, is the $n = 0$ term for which we can use the form of the transition rate found in [12] with the regulator already taken to zero, see also [11], where such singularities were also encountered and dealt with. For the $n \neq 0$ terms, the transition rate can be written as

$$\begin{aligned}\dot{\mathcal{F}}(E) &= -\frac{a^2}{2q}\sum_{n=-\infty}^{\infty}\int_{-\infty}^{\infty}\frac{\mathrm{d}r\ \mathrm{e}^{-2iEr/q}}{\sinh^2 r - \left(\frac{rp}{q}+\frac{npP}{2}\right)^2} \\ &= -\frac{a^2}{4q}\sum_{n=-\infty}^{\infty}\int_{-\infty}^{\infty}\frac{\mathrm{d}r\ \mathrm{e}^{-2iEr/q}}{\frac{rp}{q}+\frac{npP}{2}} \\ &\qquad \times\left(\frac{1}{\sinh r - \left(\frac{rp}{q}+\frac{npP}{2}\right)} - \frac{1}{\sinh r + \left(\frac{rp}{q}+\frac{npP}{2}\right)}\right), \end{aligned} \tag{7.18}$$

where the $i\epsilon$ prescription amounts to giving r a small, negative, imaginary part near the singularities on the real axis.

We evaluate (7.18) numerically. We first use Mathematica's 'FindRoot' function to solve the transcendental equations that specify the singularities in the integrand. With the singularities known, we compute the integral in (7.18) by using Mathematica's 'CauchyPrincipalValue' method of 'NIntegrate' and adding the contribution from the small semi-circle contours that pass around the singularities in the lower half-plane. The sum is cut off at some suitable value of $|n|$ when convergence has occurred to the desired precision.

8 Results

8.1 Static detector

First, we look at the numerical results for the transition rate of a static detector at fixed radius R. We use the results (5.5), (5.11) and (5.13) to numerically obtain the transition rates in the Hartle-Hawking, Boulware and Unruh states respectively.

We imposed a suitable cut-off in the ℓ-sum that increased with excitation energy (through $\tilde{\omega}$) and also increased with increasing radius, R. Considering $R = 4M$, for example, we evaluated the transition rate at the points $ME = -150/100,\ -148/100,\ \ldots,\ 148/100,\ 150/100$, excluding the $E = 0$ point. The point $E = 0$ is problematic because it would involve solving for the modes at $\omega = 0$, which proves difficult numerically. For $R = 4M$ and $M|E| = 1/100$, we cut off the ℓ-sum at $\ell = 12$, whereas at $M|E| = 150/100$ we cut off the sum

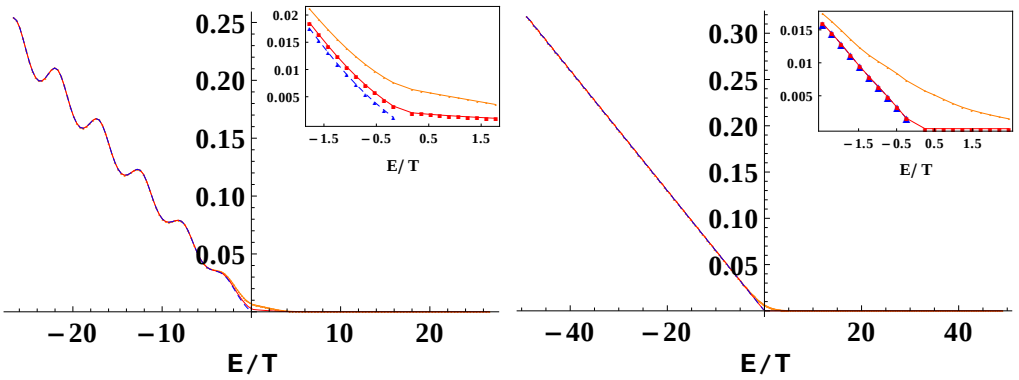

(a) $R = 4M$ (b) $R = 40M$

Figure 2: $M\dot{\mathcal{F}}$ as a function of $E/T_{\rm loc}$ for the static detector at various radii, showing the results for the Hartle-Hawking state (orange circles) computed from (5.5), Boulware state (blue dashed) computed from (5.11) and Unruh state (red solid) computed from (5.13).

at $\ell = 59$ (one could have used much lower cut-off values quite adequately here, but in the static case computation is fast and we could afford to use a larger value for the cut-off than strictly necessary). For $R = 40M$, we found that at $M|E| = 2$ a cut-off of $\ell = 107$ was more than adequate as these contributions had become negligibly small.

A final point to note is that because the differential equation (3.5) depends on ω only via ω^2, and in the static case we evaluate the modes at $\tilde{\omega} = E\sqrt{1-2M/R}$, the values of the modes $|\phi^{\rm in}_{\tilde{\omega}\ell}|^2$ and $|\phi^{\rm up}_{\tilde{\omega}\ell}|^2$ only depend on E through $|E|$. Hence, we can just evaluate over the positive range: $ME = 2/100,\ 4/100, ...,\ 150/100$, and then we immediately have the values of $|\phi^{\rm in}_{\tilde{\omega}\ell}|^2$ and $|\phi^{\rm up}_{\tilde{\omega}\ell}|^2$ over the corresponding negative energies too.

Figure 2 shows the transition rate against the excitation energy of the detector divided by the local temperature $T_{\rm loc}$ (5.6). The horizon is at $R = 2M$, and we see that as we move away from the horizon, far from the hole at $R = 40M$, the transition rates for the Boulware and Unruh states align uniformly across negative energy gap. Near the horizon, at $R = 4M$, the transition rate is seen to oscillate for large, negative energy gap. Similar oscillation was found for the BTZ hole in [11]. This oscillation appears to arise from the potential barrier in the radial equation (3.3). We show in Appendix B that similar oscillations ensue for a static detector in Minkowski spacetime when the field has an external potential with a potential wall or a potential barrier.

Given that the Unruh state represents an outgoing flux of radiation from

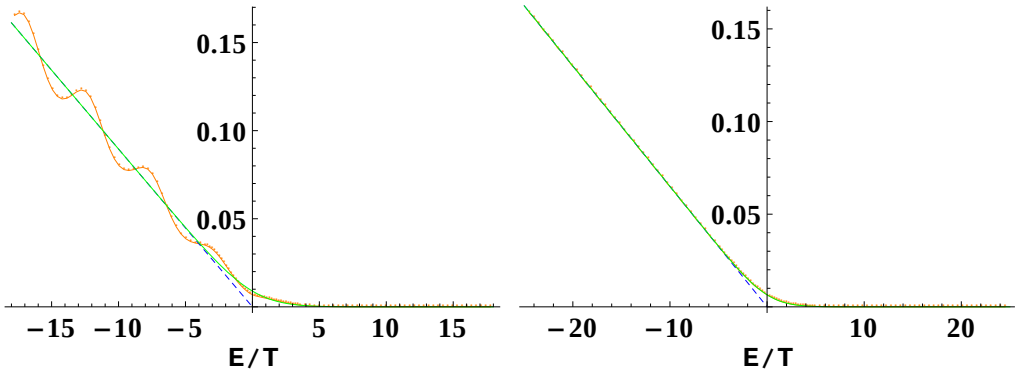

(a) $R = 4M$ (b) $R = 40M$

Figure 3: $M\dot{\mathcal{F}}$ as a function of $E/T_{\rm loc}$ for the static detector. Figure showing the results for the Hartle-Hawking state (orange circles), computed from (5.5), alongside the response rate for an inertial detector in $3+1$ Minkowski spacetime (blue dashed), $-\Theta(-E)\,E/2\pi$, and the response rate of a Rindler detector (green solid), computed from (7.2) with a proper acceleration chosen to be (7.3).

the hole, intuitively one may think that at fixed radius R external to the hole, the small-ω up-modes would be unable to escape through the potential barrier of (3.5). Thus, the reader may find it surprising that the transition rate of the static detector when the field is in the Unruh state does not go to zero as the energy gap goes to zero — implying (by the relation $\tilde{\omega} = E\sqrt{1-2M/R}$ that was encountered in Section 5) that the frequency of the modes is also being taken to zero. Because of the theta function in (5.13), the term involving the in-modes is vanishing when E is zero, but we show analytically in Appendix A that the $|\,\Phi^{\rm up}_{\omega\ell}\,|^2$ modes are proportional to ω^2 when $\omega \to 0$. Hence, this balances the $1/\big(E(\mathrm{e}^{E/T}-1)\big)$ found in the denominator and leads to a finite transition rate.

Figure 3 shows the transition rate of the static detector coupled to a scalar field in the Hartle-Hawking state compared with the transition rate of the inertial detector in 3+1 Minkowski spacetime and a Rindler detector with proper acceleration given by (7.3). First, we see that close to the hole and at large, negative energies the transition rate of the detector coupled to the scalar field in the Hartle-Hawking state, in the black hole spacetime, oscillates about that of the inertial detector, in 3+1 Minkowski spacetime. Second, we observe that as R increases, the Hartle-Hawking rate agrees to an increasing extent with the Rindler detector in flat spacetime. This is to be expected because as one moves further from the black hole the spacetime is asymptotically flat.

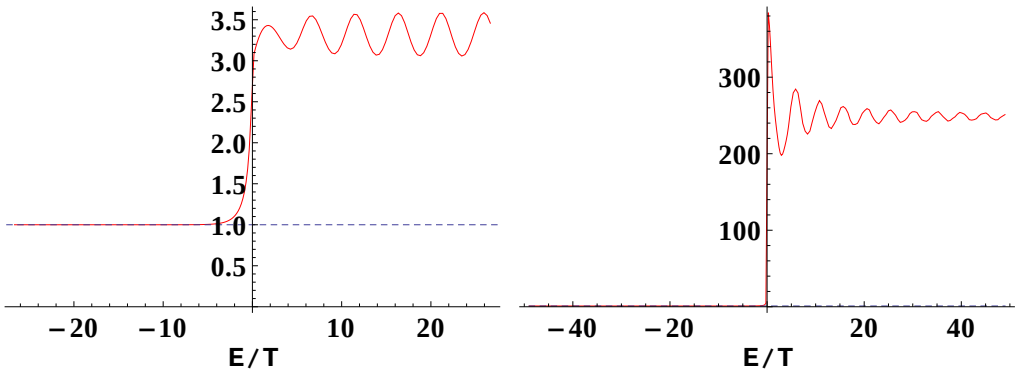

(a) $R = 4M$ (b) $R = 40M$

Figure 4: Ratio of $M\dot{\mathcal{F}}$, as a function of E/T_{loc}, for the static detector in the Hartle-Hawking state to that of the static detector in the Unruh state. The discontinuity near the origin is caused by the numerical difficulty in computing the modes at small ω.

Figure 4 shows the ratio of the transition rate of the static detector coupled to a field in the Hartle-Hawking state to the transition rate of the same detector coupled to a field in the Unruh state. We see that this ratio becomes larger at positive excitation energies and when the radius increases. The Unruh state represents a radiating black hole and this radiation will die off by an r^{-2} power law, whereas the Hartle-Hawking state represents a constant heat bath at spatial infinity; therefore, it is to be expected that the ratio between the Hartle-Hawking and Unruh states becomes large as $R \to \infty$. The discontinuity that appears in the curves of Figure 4 is a numerical artefact caused by the fact that solving the ODE (3.5) becomes difficult for small ω. By the relation $\tilde{\omega} = E\sqrt{1-2M/R}$ that we found in Section 5, this means computing the transition rate near $E = 0$ is difficult and we did not attempt this.

To investigate thermality, we look at the quantity

$$T_a := E/\log\left(\dot{\mathcal{F}}(-E)/\dot{\mathcal{F}}(E)\right). \tag{8.1}$$

When the KMS condition is satisfied, T_a (8.1) is independent of E and equal to the temperature. As noted in (5.7), this is what happens for the Hartle-Hawking state, with $T_a = T_{\text{loc}}$. Figure 5 shows T_a as a function of E/T_{loc} for the Hartle-Hawking state and for the Unruh state. For the Unruh state, the plot shows that $T_a \to T_{\text{loc}}$ as E increases. This means that in the limit of a large energy gap, the detector's response in the Unruh state becomes approximately thermal at the local Hawking temperature T_{loc}.

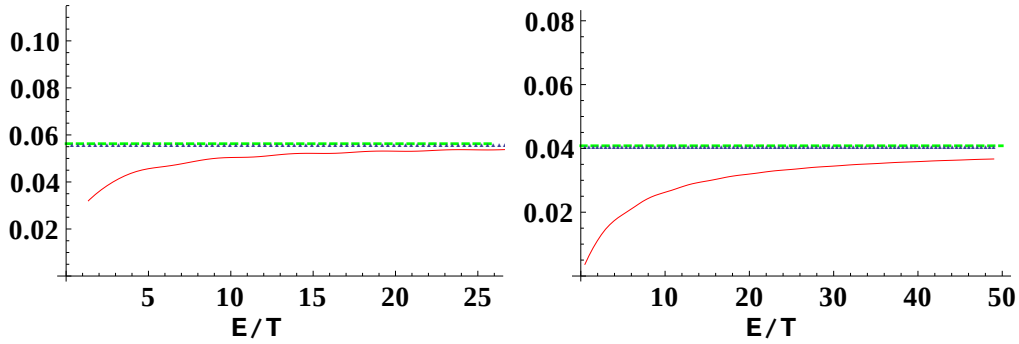

(a) $R = 4M$ (b) $R = 40M$

Figure 5: Figure shows T_a (8.1) as a function of E/T_{loc} for a static detector. The thick, green, dashed line is the local Hawking temperature T_{loc}. The line with blue triangles is the numerically computed T_a for the Hartle-Hawking state, showing agreement with the analytic result $T_a = T_{\text{loc}}$. The solid red curve is the numerically computed T_a for the Unruh state.

8.2 Circular detector results

In this section, we present the results obtained for the detector on a circular-geodesic in Schwarzschild spacetime. These results are computed from the numerical evaluation of the transition rates (6.5), (6.9) and (6.13).

For the circular-geodesic detector's transition rate, we had the double ℓ-, m-sum to compute, but as we noted in Section 6, we can demand that $m \equiv \ell (\text{mod} 2)$ to reduce the workload by half. We cut off the ℓ-sum in the transition rate when the contributions at large ℓ become negligible. As with the static case, this cut-off is increased as ω or R increases. Note that for computational efficiency one can take the ℓ cut-off of the $\Phi_{\omega_-,\ell}$ modes at a significantly lower value than the ℓ cut-off for the $\Phi_{\omega_+,\ell}$ modes (for both up- and in-modes).

Figure 6 shows the transition rate against the excitation energy of the detector, made dimensionless by the multiplication by the mass of the black hole, M. The horizon is at $R = 2M$, and we see that as we move away from the horizon, far from the hole at $R = 40M$, the transition rates for the Boulware and Unruh states align for negative excitation energies. Below $R = 6M$, the circular orbits are unstable but this seems to have no qualitative effect on the transition rate of the detector. Near the hole and for sufficiently large, negative energy gap, the Hartle-Hawking and Unruh rates align, but in the circular case, even at large, negative energies, the Boulware rate does not align with the Hartle-Hawking and Unruh rates.

Figure 7 shows the transition rate of the detector on the Schwarzschild

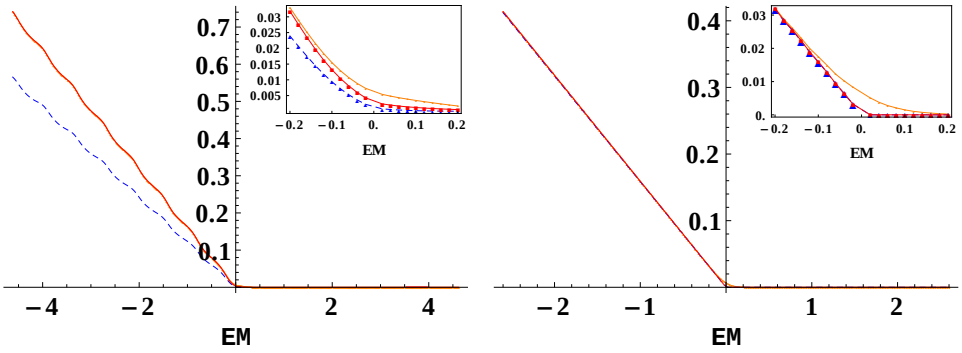

(a) $R = 4M$ (b) $R = 40M$

Figure 6: $M\dot{\mathcal{F}}$ as a function of EM for the circular detector. The figure shows the transition rate for the Hartle-Hawking state (orange circles) computed from (6.5), Boulware state (blue dashed) computed from (6.9) and Unruh state (red solid) computed from (6.13).

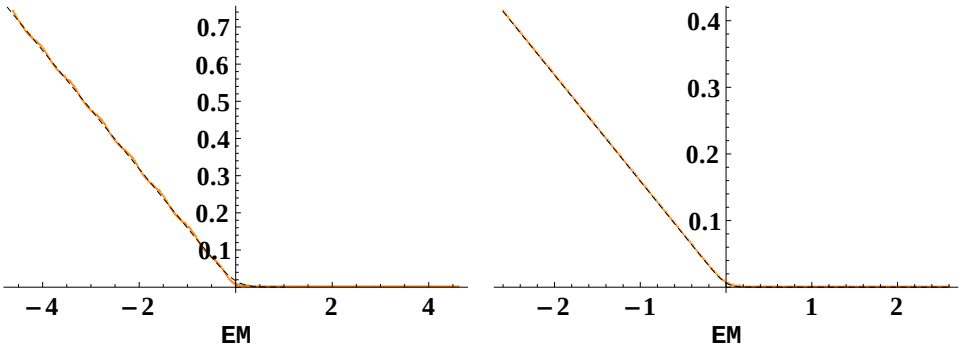

(a) $R = 4M$ (b) $R = 40M$

Figure 7: $M\dot{\mathcal{F}}$ as a function of EM for the circular detector, compared with the Rindler detector with transverse drift. The figure shows the transition rate for the Hartle-Hawking state (orange circles), computed from (6.5), alongside the transition rate rate for a Rindler detector with transverse drift (black-dashed). The Rindler rate is computed by substituting the interval (7.14) into the regulator-free transition rate found in [12] and then numerically evaluating.

black hole coupled to a scalar field in the Hartle-Hawking state compared with a detector in Rindler spacetime, moving on a Rindler trajectory but drifting with constant velocity in the transverse dimension; that is to say, the trajectory is given by (7.5), with (7.6), (7.12) and (7.13). We see that as the radius R increases the agreement becomes better. As $R \to \infty$, the circular detector is becoming asymptotically a static detector, so the agreement should not be surprising considering our results in Section 8.1. Near the hole, at $R = 4M$ the transition rate in the Hartle-Hawking state appears to oscillate around that of the drifting Rindler detector when the energy gap is large and negative.

Figure 8 shows the results that we obtained by making the transverse direction that the drifting Rindler detector's drift occurs in periodic, such that the period matches the period in proper time needed for the circular-geodesic detector, in Schwarzschild spacetime, to complete an orbit. The method of images sum (7.18) was cut off at $|n| = 500$, by which point the sum had converged. We see by comparing Figures 7a and 7b with Figure 8 that the agreement with the Schwarzschild detector is actually made worse by enforcing periodicity. We note that the oscillation at large, negative energies seen in Figure 8 is reminiscent of that seen for the co-rotating detector in the BTZ spacetime in [11].

Figure 9 shows the ratio of the transition rate of the detector on a circular geodesic coupled to a field in the Hartle-Hawking state, to the transition rate of the circular-geodesic detector coupled to a field in the Unruh state. We see that just like in the static case, this ratio becomes larger at positive excitation energies and when the radius increases.

Finally, we ask whether the response is thermal in the sense of the KMS property. By the discussion at the end of Section 8.1, this amounts to examining whether the quantity T_a (8.1) is constant.

Plots of T_a as a function of EM are shown in Figure 10. Assuming that the range of EM in the plots is representative, we see that T_a appears to level off as EM increases, both for the Hartle-Hawking state and for the Unruh state. The data does not extend to high enough EM for the asymptotic values of T_a to be read off with accuracy, but the $R = 4M$ plot strongly suggests that the asymptotic value for each state is higher than the local Hawking temperature T_{loc} (5.6), and also higher than the Doppler-shifted local Hawking temperature,

$$T_{\text{Doppler}} := (-\mathsf{U}_{\text{static}} \cdot \mathsf{U}_{\text{circ}})\, T_{\text{loc}} \ . \tag{8.2}$$

The $R = 40M$ plot supports a similar conclusion for the Hartle-Hawking state but remains inconclusive for the Unruh state.

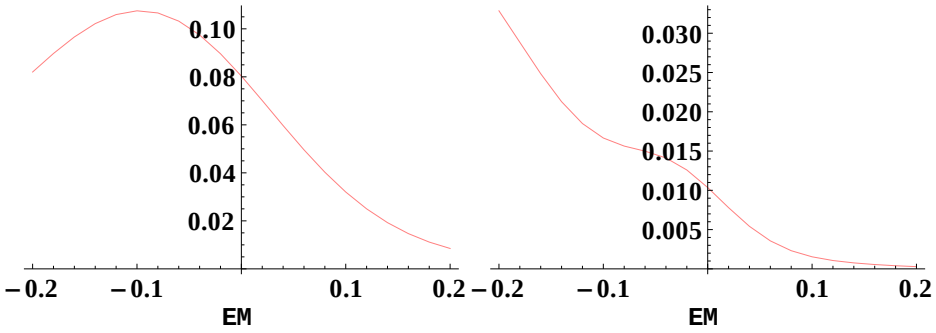

(a) $R = 4M$ (b) $R = 40M$

Figure 8: Transition rate of a Rindler detector with drift in the transverse direction where the transverse direction has been periodically identified. Computed from (7.18) with $|n|$ cut off at 500.

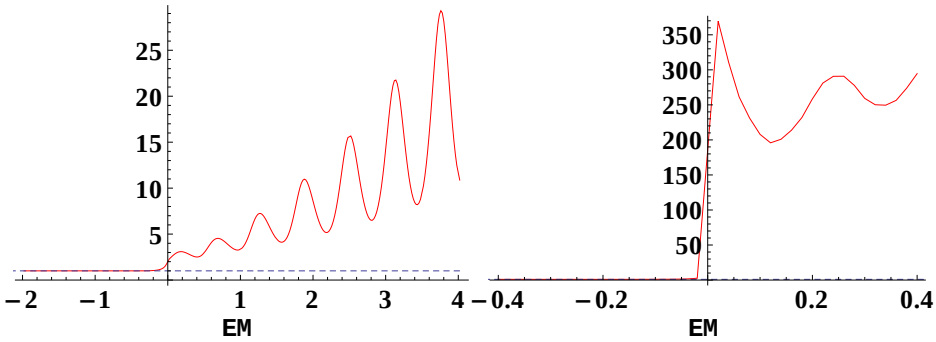

(a) $R = 4M$ (b) $R = 40M$

Figure 9: Ratio of $M\dot{\mathcal{F}}$, as a function of EM, for the circular-geodesic detector in the Hartle-Hawking state, to the transition rate of the circular-geodesic detector in the Unruh state. The discontinuity that appears near the origin is a numerical artefact owing to the fact that solving the ODE (3.5) becomes difficult at small ω.

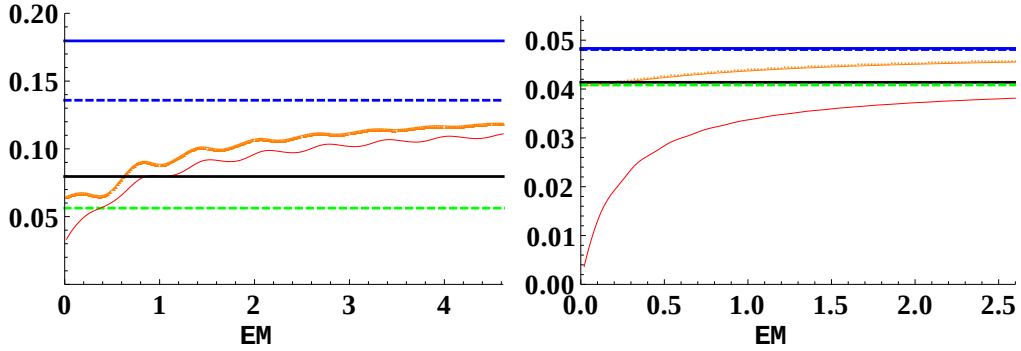

(a) $R = 4M$ (b) $R = 40M$

Figure 10: Figure shows T_a (8.1) as a function of EM for the circular-geodesic detector, in orange circles for the Hartle-Hawking state and in solid red for the Unruh state. The horizontal dashed thick green line is the local Hawking temperature $T_{\rm loc}$ (5.6), and the horizontal solid thick black line is the Doppler-shifted local Hawking temperarature $T_{\rm Doppler}$ (8.2). Finally, the horizontal solid and dashed blue lines are obtained by shifting $T_{\rm loc}$ by respectively the factors (C.7) and (C.12) that arise in similar situations involving a drift velocity in Minkowski space, as shown in Appendix C.

These results for T_a at a large energy gap are similar to what we find in Appendix C for the response of a detector in Minkowski spacetime in three stationary situations where the detector has a nonvanishing velocity with respect to a family of detectors whose response is exactly KMS. The physical explanation for a blueshift above the Doppler shift appears to be that while the Doppler shift in (8.2) is due to just the time dilation, the transition rate at large excitation energies is dominated by the most energetic field quanta, and these are seen by the detector from a head-on direction and are hence blueshifted more than just by time dilation. This explanation is consistent with the analysis of a circular-geodesic detector in [28] within a model in which the angular dependence of the field is suppressed, where it was found that the asymptotic temperature in a state closely resembling the Unruh state is related to the local Hawking temperature by just the time dilation Doppler shift factor.

9 Summary and concluding remarks

In this paper, we have analysed the response of an Unruh-DeWitt detector coupled to a massless scalar field on the four-dimensional Schwarzschild black hole using numerical methods.

For the static detector in the exterior region, we analysed the response when the field was in the Hartle-Hawking, Boulware and Unruh states. At a variety of radii, the results were presented in the form of plots of the detector's transition rate, plotted against the detector's energy gap scaled by the local Hawking temperature. For the field in the Hartle-Hawking state, we verified that the response of the detector was thermal, in the KMS sense, with local temperature given by $T_{\text{loc}} = 1/\big(8\pi M\sqrt{1-2M/R}\,\big)$, as known from the complex analytic properties of the Wightman function. For a static detector and with the field in the Boulware state, the plots showed that the response of the detector consists only of de-excitation and that the excitation rate is vanishing; this is consistent with the fact that the static detector is on an orbit of the ∂_t Killing vector, where t is the Schwarzschild time co-ordinate. We also observed from the plots that as the radius increased, the Boulware and Unruh rates tended to become equal. This is consistent with the fact that the Unruh rate represents an outgoing flux of radiation from the hole that diminishes by r^{-2} as the radius, r, tends to infinity, combined with the fact that the Boulware state tends to the Minkowski vacuum as the radius tends to infinity. The Hartle-Hawking state represents a thermal heat bath as the radius tends to infinity, and we plotted the ratio of the transition rate in the Hartle-Hawking state to the transition rate in the Unruh state, for the static detector, finding that the ratio of the excitation rates increases rapidly with radius. We found that for a large energy gap the transition rate in the Unruh state became approximately thermal, and the detector recorded the local Hawking temperature.

We also presented results for a detector on a variety of circular geodesics, stable and unstable. The results were once again in the form of plots of the transition rate against the detector's energy gap, this time scaled to be dimensionless by multiplying by the mass of the black hole, M. Results were presented in the Hartle-Hawking, Boulware and Unruh states. The stability of the orbit seemed to have no qualitative effect on the transition rate. The Boulware state in this case has a non-vanishing excitation component, and this component increases as the radius decreases. This is consistent with the fact that at large radius the circular-geodesic detector asymptotes to a static detector, so the detector becomes approximately on a ∂_t orbit, but at small radius the detector is no longer on such an orbit, and there is room for positive energy excitations to occur. Similarly to the static case, the circular-geodesic plots also show that as the radius increases, the Boulware and Unruh states tend to become equal and that the ratio of the Hartle-Hawking rate to Unruh rate becomes large.

In the limit of a large energy gap, we found evidence that the response of a circular-geodesic detector in both the Hartle-Hawking state and the Unruh

state becomes thermal in the KMS sense, in a temperature that is higher than the local Hawking temperature, by a factor that is genuinely larger than the Dopper blueshift factor due to the velocity of the circular geodesic with respect to the static detectors. This is consistent with the response of a detector in three qualitatively similar stationary situations in Minkowski spacetime, as we shall show in Appendix C. The physical explanation appears to be that the transition rate at large excitation energies is dominated by the most energetic field quanta, and these are seen by the detector from a head-on direction and are hence blueshifted more than by the Doppler shift factor that accounts for just the time dilation. This explanation is consistent with the analysis of a circular-geodesic detector in [28] within a model in which the angular dependence of the field is suppressed, where the asymptotic temperature in a state closely resembling the Unruh state was found to be related to the local Hawking temperature by just the time dilation Doppler shift factor.

Finally for the static detector coupled to a field in the Hartle-Hawking state, a comparison was made to the plot of the transition rate of the Rindler detector in the Minkowski vacuum, with the proper acceleration chosen appropriately. Similarly, for the circular-geodesic detector a comparison was made to a Rindler detector with appropriately chosen proper acceleration, but this time also given a constant velocity drift in the transverse direction; the idea was that this would serve as an analogue to the angular motion of the circular geodesic. The results in both cases showed that as the radius increased, the Hartle-Hawking and Rindler rates aligned. At smaller radius, the Hartle-Hawking rate appears to oscillate about the Rindler (or drifting Rindler) rate.

All the situations analysed were stationary, and we relied on this stationarity at the outset in order to extract from the formally divergent total transition probability a finite transition probability per unit time. While this procedure has a long pedigree [1], it would not be applicable in non-stationary situations, such as a detector falling into a black hole [28, 36]. For our Schwarzschild Wightman functions that are given in terms of mode sums, integration over the detection time for a nonstationary trajectory will no longer collapse the integral over ω, and the task of evaluating the transition rate numerically becomes significantly more involved. In particular, the Wightman function is divergent at short distances, and while it is known how the divergent parts come to be subtracted in the expressions for the transition probability and transition rate [14], the challenge in numerical work is to implement these subtractions term by term in a mode sum. For a radially infalling geodesic in Schwarzschild, a subtraction procedure in the Hartle-Hawking state is presented in [37], and a numerical evaluation of the

transition rate is in progress. We hope to report on the results of this evaluation in a future paper.

Acknowledgements

We have benefited from discussions with numerous colleagues, including Benito Juárez-Aubry, Sanved Kolekar, Robb Mann, Eduardo Martín-Martínez, Eric Poisson, Suprit Singh, Matteo Smerlak and Bill Unruh. L.H. thanks Bill Unruh for hospitality at the University of British Columbia during a Universitas 21 Prize Scholarship visit. The numerical work was made possible by access to the University of Nottingham High Performance Computing Facility. L.H. was supported by EPSRC through a PhD Studentship and a PhD Plus Fellowship at the University of Nottingham. J.L. was supported in part by STFC (Theory Consolidated Grant ST/J000388/1). A.C.O. acknowledges support from Science Foundation Ireland under Grant No. 10/RFP/PHY2847.

A Appendix: Small-ω behaviour of radial up-modes.

In this appendix, we show that at small ω the up-modes are proportional to ω. The technique overlaps with that in the Appendix of [38] but using the Whittaker equation (A.3) allows us to introduce a solution basis that remains manifestly regular for non-negative integer ℓ.

First, define the dimensionless quantities $x := r/(2M) - 1$ and $k = 2M\omega$. In terms of these variables, the radial equation (3.5) reads

$$\left[\frac{d^2}{dx^2} + \frac{(2x+1)}{x(x+1)}\frac{d}{dx} + k^2\left(\frac{x+1}{x}\right)^2 - \frac{\ell(\ell+1)}{x(x+1)}\right]\Phi_{\omega\ell} = 0\,, \tag{A.1}$$

where $x > 0$.

In the region $x \gg k+1$, we do a large-x Taylor expansion, keeping terms up to and including $O\left(x^{-2}\right)$, resulting in

$$\left[\frac{d^2}{dx^2} + \frac{2}{x}\frac{d}{dx} + k^2\left(\frac{x+1}{x}\right)^2 - \frac{\ell(\ell+1)}{x^2}\right]\Phi_{\omega\ell} = 0\,. \tag{A.2}$$

By writing $\Phi_{\omega\ell} = P/x$ followed by the change of variables $z = 2ikx$, equation (A.2) reduces to

$$\left[\frac{d^2}{dz^2} + \left(-\frac{1}{4} - \frac{ik}{z} + \frac{k^2 - \ell(\ell+1)}{z^2}\right)\right]P = 0\,. \tag{A.3}$$

This is the Whittaker equation, (13.14.1) of [33], with

$$\begin{aligned} K &= ik\,, \\ \mu &= \sqrt{(\ell+1/2)^2 - k^2}\,. \end{aligned} \tag{A.4}$$

Including a suitably chosen phase factor, the general solution of (A.3) leads to [33]

$$\begin{aligned} \Phi_{\omega\ell} = {} & D_1 \frac{\mathrm{e}^{-ikx}}{x}(2ikx)^{\mu+1/2} M\left(\mu+ik+1/2, 1+2\mu, 2ikx\right) \\ & + D_2 \frac{\mathrm{e}^{-ikx}}{x}(2ikx)^{\mu+1/2} U\left(\mu+ik+1/2, 1+2\mu, 2ikx\right)\,, \end{aligned} \tag{A.5}$$

where D_1 and D_2 are constants.

To determine D_1 and D_2 we compare (A.5) with the $r \to \infty$ asymptotic form of the up-modes, (3.16) (now remembering to include the $1/(2M)$ normalisation factor of (3.21)). After determination of these coefficients, we find that (A.5) reads

$$\begin{aligned} \Phi^{\mathrm{up}}_{\omega\ell} = {} & \frac{B^{\mathrm{up}}_{\omega\ell}}{(2M)^2} \frac{\Gamma\left(\mu+ik+1/2\right)}{x}\, \mathrm{e}^{ik}(2ik)^{-ik}\,(2ikx)^{\mu+1/2}\,\mathrm{e}^{-ikx} \\ & \times \Bigg[\frac{M\left(\mu+ik+1/2, 1+2\mu, 2ikx\right)}{\Gamma\left(1+2\mu\right)} \\ & \qquad - \frac{\mathrm{e}^{i\pi(\mu+ik+1/2)}}{\Gamma\left(\mu-ik+1/2\right)} U\left(\mu+ik+1/2, 1+2\mu, 2ikx\right) \Bigg]\,. \end{aligned} \tag{A.6}$$

Next, we look at the limiting form of (A.6) at $1 \ll x \ll (\ell+1)/k$; in other words, the limit under consideration is that of large, fixed $x \gg 1$, whilst $k \to 0$. Hence, expanding in small kx, we find, using (13.2.16), (13.14.4) and (13.14.6) of [33], that to leading order

$$\begin{aligned} \Phi^{\mathrm{up}}_{\omega\ell} &= \frac{B^{\mathrm{up}}_{\omega\ell}}{(2M)^2 x}(-1)^{\ell}\frac{(2\ell)!}{\ell!}k^{-ik}(2ikx)^{-\ell} \\ &= \frac{B^{\mathrm{up}}_{\omega\ell}}{(2M)^2 x}(-1)^{\ell}\frac{(2\ell)!}{\ell!}(2ikx)^{-\ell}\,. \end{aligned} \tag{A.7}$$

Finally, using the small-ω result for the transmission coefficient, $B^{\mathrm{up}}_{\omega\ell}$, given in [39], we obtain

$$\Phi_{\omega\,,\ell=0} = \frac{1}{2Mx}\,(-2ik) \tag{A.8}$$

which establishes that for $\ell = 0$, $\Phi_{\omega\,,\ell=0} \sim \omega$ as $\omega \to 0$.

B Appendix: Potential barrier leads to oscillations in the transition rate

In this appendix we discuss two analytically solvable systems with a potential barrier. In both systems we show that the detector's de-excitation rate depends on the detector's energy gap in a way that involves a superposition of linear and oscillatory behaviour. This is in agreement with the results found numerically for the detector in the Schwarzschild spacetime in the main text.

We consider a scalar field in (3+1)-dimensional Minkowski spacetime, and we work in a set of standard Minkowski coordinates (t, x, y, z). We assume that the field is massless but the wave equation has an external potential $V(x)$ that depends on x but not on t, y or z, such that the spectrum of the operator $-(\partial_x^2+\partial_y^2+\partial_z^2)+V$ is the positive continuum. The wave equation is then separable, and the solutions that have positive frequency with respect to ∂_t take the form

$$\phi_{\alpha\kappa_y\kappa_z}(t,x,y,z) = \frac{1}{\sqrt{16\pi^3\omega_\alpha}}\,\mathrm{e}^{-i\omega_\alpha t+i\kappa_y y+i\kappa_z z}\;u_\alpha(x) \tag{B.1}$$

where κ_y and κ_z are real-valued, α is a (multi-)index that labels the solutions u_α to the one-dimensional wave equation

$$-\frac{\mathrm{d}^2u_\alpha}{\mathrm{d}x^2} + V(x)u_\alpha(x) = \lambda_\alpha^2 u_\alpha(x) \tag{B.2}$$

where we may choose $\lambda_\alpha > 0$ without loss of generality, and ω_α is the positive solution to the dispersion relation

$$\omega_\alpha^2 = \lambda_\alpha^2 + \kappa^2 \tag{B.3}$$

with $\kappa = (\kappa_y^2+\kappa_z^2)^{1/2}$. We take the solutions u_α to be normalised as

$$\int u_\alpha(x)u_\beta^*(x)\,\mathrm{d}x = 2\pi\delta_{\alpha\beta}\ , \tag{B.4}$$

where $\delta_{\alpha\beta}$ stands for the Dirac delta-function in the continuous components of the (multi-)indices α and β and for a Kronecker delta in any discrete components of the (multi-)indices. It follows that the solutions $\phi_{\alpha\kappa_y\kappa_z}$ (B.1) are then (Dirac) orthonormal in the Klein-Gordon inner product, and we may Fock quantise the field in the usual fashion.

In the vacuum with respect to ∂_t, the transition rate of a stationary

detector at $x = x_0$ takes the form

$$\begin{aligned}
\dot{\mathcal{F}}(E) &= \int \mathrm{d}\mu(\alpha) \int_0^\infty \mathrm{d}\kappa\kappa \, \frac{\delta(E+\omega_\alpha)}{4\pi\omega_\alpha} \, |u_\alpha(x_0)|^2 \\
&= \int \mathrm{d}\mu(\alpha) \int_0^\infty \mathrm{d}\kappa\kappa \frac{\delta\big(E+(\lambda_\alpha^2+\kappa^2)^{1/2}\big)}{4\pi(\lambda_\alpha^2+\kappa^2)^{1/2}} \, |u_\alpha(x_0)|^2 \\
&= \frac{1}{4\pi} \int \mathrm{d}\mu(\alpha) \int_{\lambda_\alpha}^\infty \mathrm{d}s \, \delta(E+s) \, |u_\alpha(x_0)|^2 \\
&= \frac{\theta(-E)}{4\pi} \int \mathrm{d}\mu(\alpha) \theta(-E-\lambda_\alpha) \, |u_\alpha(x_0)|^2 \ , \qquad \text{(B.5)}
\end{aligned}$$

where $\mathrm{d}\mu(\alpha)$ denotes the spectral measure in the (multi-)index α.

We now apply (B.5) to the well known case of a free field in Minkowski space [5], to the infinite half-space potential wall [40] and to the repulsive Pöschl-Teller potential.

B.1 Free field: no potential barrier

For the free field in Minkowski space, we have $V(x) = 0$, $\alpha = k \in \mathbb{R}$, $u_k(x) = e^{ikx}$ and $\lambda_k = |k|$. From (B.5), we obtain

$$\begin{aligned}
\dot{\mathcal{F}}_{\mathrm{M}}(E) &= \frac{\theta(-E)}{4\pi} \int_{-\infty}^\infty \mathrm{d}k \, \theta(-E-|k|) \\
&= -\frac{E}{2\pi} \, \theta(-E) \ , \qquad \text{(B.6)}
\end{aligned}$$

which is the well-known result [5].

B.2 Half-space: infinite potential barrier

For a free field confined to the half-space $x > 0$, we have $V(x) = 0$ for $x \geq 0$, and we may think of the potential as an infinite wall, so that $V(x) = \infty$ for $x < 0$. With Dirichlet or Neumann boundary conditions at $x = 0$, we then have $\alpha = k \in \mathbb{R}_+$,

$$u_k(x) = \begin{cases} 2\sin(kx) & \text{for Dirichlet;} \\ 2\cos(kx) & \text{for Neumann,} \end{cases} \qquad \text{(B.7)}$$

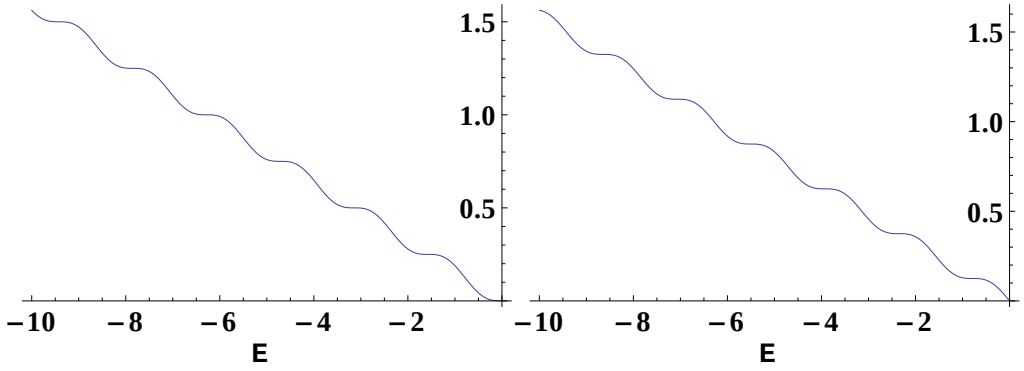

(a) $\eta = -1$ (b) $\eta = 1$

Figure 11: $\dot{\mathcal{F}}$ as a function of E for a free field in a half-space, computed from (B.8) at $x_0 = 2$ for both Dirichlet ($\eta = -1$) and Neumann ($\eta = 1$) boundary conditions.

and $\lambda_k = k$. For a static detector at $x = x_0 > 0$, (B.5) gives

$$\begin{aligned}\dot{\mathcal{F}}_{\text{wall}}(E) &= \frac{\theta(-E)}{4\pi}\int_0^\infty \mathrm{d}k\,\theta(-E-k)\,|u_k(x_0)|^2 \\ &= \frac{\theta(-E)}{4\pi}\int_0^{-E} \mathrm{d}k\,|u_k(x_0)|^2 \\ &= \frac{1}{2\pi}\left(-E - \eta\frac{\sin(2Ex_0)}{2x_0}\right)\theta(-E)\ , \end{aligned} \tag{B.8}$$

where $\eta = -1$ for Dirichlet and $\eta = 1$ for Neumann. This result was obtained in [40] by the method of images.

The transition rate (B.8) is the superposition of the Minkowski rate (B.6), linear in E, and a term that is oscillatory in E with period π/x_0. Plots are shown in Figure 11.

B.3 Pöschl-Teller potential: smooth potential barrier

As an example of a smooth potential barrier, we consider the repulsive Pöschl-Teller potential,

$$V(x) = \frac{\frac{1}{4} + \mu^2}{\cosh^2 x}\ , \tag{B.9}$$

where $\mu^2 > -\frac{1}{4}$. This potential is exactly solvable, and it provides a good approximation to the potential in the Schwarzschild radial equation (3.3).

We note in passing that the radial equation for massless wave propagation in the Nariai spacetime [41, 42] can be shown to have exactly the Pöschl-Teller form (B.9). This suggests that the Nariai spacetime can provide insight into wave propagation in Schwarzschild.

With the Pöschl-Teller potential (B.9), we may choose the normalised solutions to (B.2) to be

$$u_k^{\text{in}}(x) = \sqrt{\frac{k\pi \sinh k\pi}{\cosh^2(\pi\mu) + \sinh^2(\pi k)}}\, \mathrm{P}^{ik}_{-(1/2)+i\mu}(-\tanh x) \ , \tag{B.10a}$$

$$u_k^{\text{up}}(x) = \sqrt{\frac{k\pi \sinh k\pi}{\cosh^2(\pi\mu) + \sinh^2(\pi k)}}\, \mathrm{P}^{ik}_{-(1/2)+i\mu}(\tanh x) \ , \tag{B.10b}$$

where $k > 0$, P is the associated Legendre function defined with argument on the interval $(-1, 1)$ by (14.3.1) in [33], and $\lambda_k = k$. The superscripts "in" and "up" follow the black hole terminology, in the sense that u_k^{in} is proportional to e^{-ikx} at $x \to -\infty$ and u_k^{up} is proportional to e^{ikx} at $x \to \infty$. The normalisation in (B.10) can be verified by considering the asymptotic behaviour at $x \to \pm\infty$ [43].

For a static detector at $x = x_0$, (B.5) gives

$$\begin{aligned} \dot{\mathcal{F}}_{\text{PT}}(E) &= \frac{\theta(-E)}{4\pi} \int_0^\infty \mathrm{d}k\, \theta(-E-k) \, \left(|u_k^{\text{in}}(x_0)|^2 + |u_k^{\text{up}}(x_0)|^2 \right) \\ &= \frac{\theta(-E)}{4\pi} \int_0^{-E} \mathrm{d}k \, \left(|u_k^{\text{in}}(x_0)|^2 + |u_k^{\text{up}}(x_0)|^2 \right) \ . \end{aligned} \tag{B.11}$$

A plot of the transition rate (B.11) is shown in Figure 12. For small $|E|$ the potential acts as a reflective wall, and the transition rate superposes oscillatory behavour in E on the linear behaviour of the free field. For large $|E|$ the potential wall becomes irrelevant and the transition rate asymptotes to that of the free field.

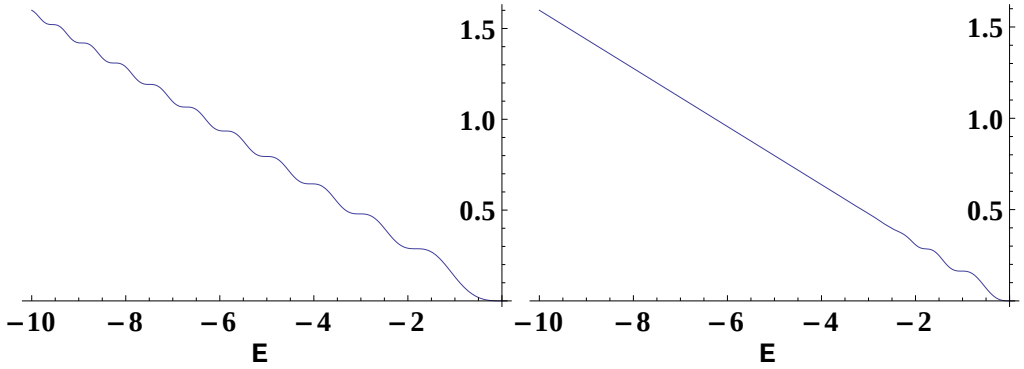

(a) $\mu = 10$, $x_0 = 4$ (b) $\mu = 2$, $x_0 = 4$

Figure 12: $\dot{\mathcal{F}}$ as a function of E in the Pöschl-Teller potential, computed from (B.11), in (a) with $\mu = 10$ and $x_0 = 4$, and in (b) with $\mu = 2$ and $x_0 = 4$.

C Appendix: Asymptotic large energy KMS for stationary worldlines in Minkowski space

In this appendix we show that the KMS condition holds asymptotically in the large energy limit for three stationary detector worldlines in $(3 + 1)$-dimensional Minkowski spacetime, in situations where the detector has a nonvanishing velocity with respect to a reference trajectory for which the KMS condition holds exactly. In all three cases the asymptotic KMS temperature is larger than the reference KMS temperature, by a factor that exceeds the time dilation Doppler shift factor that might be expected on kinematical grounds.

These analytic results are in qualitative agreement with the numerical results found in the main text for the transition rate of a detector on a circular geodesic in Schwarzschild.

We work throughout the appendix in $(3 + 1)$-dimensional Minkowski spacetime. We follow the notation of Section 7 and denote a standard set of Minkowski coordinates by (t, x, y, z).

C.1 Rindler with transverse drift in Minkowski vacuum

We consider a detector on the trajectory (7.5),

$$\mathsf{x}(\tau)_{\text{drift}} = \frac{1}{a}\big(\sinh(q\tau), \cosh(q\tau), p\tau, 0\big) , \tag{C.1}$$

where $a > 0$, $p > 0$, $q = \sqrt{a^2 + p^2}$, and τ is the proper time. This trajectory is stationary, following an orbit of the Killing vector $q(t\partial_x + x\partial_t) + (p/a)\partial_y$. Setting $p = 0$ yields a Rindler trajectory of proper acceleration a: compared with this reference Rindler trajectory, our trajectory (C.1) has a constant drift velocity $v = p/q$. A pair of independent parameters is for example (a, v), where $a > 0$ and $0 < v < 1$. Alternatively, we may express v in terms of the rapidity λ by $v = \tanh\lambda$ and use the pair (a, λ), where $a > 0$ and $\lambda > 0$.

We take the field to be in the Minkowski vacuum. With switch-on and switch-off pushed to infinity, the stationary transition rate can be written as [12]

$$\dot{\mathcal{F}}(E) = \dot{\mathcal{F}}^{\text{inertial}}(E) + \dot{\mathcal{F}}^{\text{corr}}(E) , \tag{C.2}$$

where

$$\dot{\mathcal{F}}^{\text{inertial}}(E) = -\frac{E}{2\pi}\Theta(-E) , \tag{C.3a}$$

$$\dot{\mathcal{F}}^{\text{corr}}(E) = \frac{1}{2\pi^2}\int_0^\infty \mathrm{d}s \cos(Es)\left(\frac{1}{(\Delta\mathsf{x})^2} + \frac{1}{s^2}\right) . \tag{C.3b}$$

Substituting (C.1) in (C.3b) and introducing the new integration variable z by $s = (2/q)z$, we find

$$\dot{\mathcal{F}}^{\text{corr}}(E) = \frac{a^2}{8\pi^2 q}\int_{-\infty}^{\infty} \mathrm{d}z\ \mathrm{e}^{2iz|E|/q}\left(\frac{1}{(1-v^2)\,z^2} - \frac{1}{\sinh^2 z - v^2 z^2}\right) . \tag{C.4}$$

To find the leading behaviour of $\dot{\mathcal{F}}^{\text{corr}}(E)$ at large $|E|$, we first deform the integration in (C.4) to a contour C that passes $z = 0$ in the upper half of the complex z plane. With this contour, the contribution from the first term in the integrand vanishes and we have

$$\dot{\mathcal{F}}^{\text{corr}}(E) = -\frac{a^2}{8\pi^2 q}\int_C \frac{\mathrm{e}^{2iz|E|/q}\,\mathrm{d}z}{\sinh^2 z - v^2 z^2} . \tag{C.5}$$

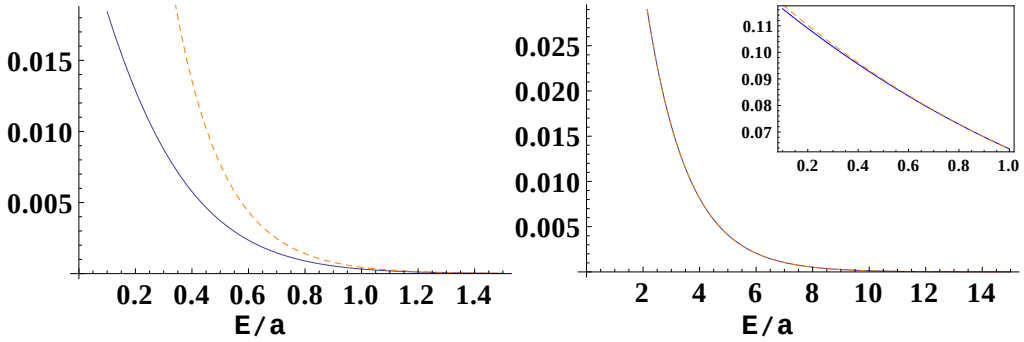

(a) $v = 0.1$ (b) $v = 0.9$

Figure 13: The solid (blue) lines show the noninertial correction $\dot{\mathcal{F}}^{\rm corr}$ (C.4) to the transition rate of the Rindler detector with a transverse drift. With $\dot{\mathcal{F}}^{\rm corr}/a$ on the vertical axis and E/a on the horizontal axis, the dimensionful parameter a becomes scaled out and the graph depends only on the dimensionless parameter v: the two plots show respectively (a) $v = 0.1$ and (b) $v = 0.9$. The dashed (red) curves show the asymptotic large energy approximation (C.6).

A standard set of contour deformation arguments shows that the integral in (C.5) equals $2\pi i$ times the sum of the residues of the poles in the upper half-plane. The dominant contribution at $|E| \to \infty$ comes from the pole with the smallest imaginary part, which is at $z = iy_+$, where y_+ is the unique solution to the transcendental equation $\sin y = vy$ in the interval $0 < y < \pi$. We thus have

$$\dot{\mathcal{F}}^{\rm corr}(E) \sim \frac{a^2 \exp(-2|E|y_+/q)}{8\pi q v y_+ (v - \cos y_+)} , \qquad |E| \to \infty . \tag{C.6}$$

A numerical comparison of $\dot{\mathcal{F}}^{\rm corr}(E)$ and the asymptotic approximation (C.6) is shown in Figure 13.

From (C.2), (C.3a) and (C.6) it follows that $\dot{\mathcal{F}}(E)$ satisfies at $|E| \to \infty$ the KMS condition (5.7) at the temperature $T_{\rm R+drift} = q/(2y_+)$. The KMS temperature of the $v \to 0$ Rindler trajectory is $T_{\rm Rindler} = a/(2\pi)$. Hence

$$\frac{T_{\rm R+drift}}{T_{\rm Rindler}} = \frac{\pi}{y_+} \cosh\lambda . \tag{C.7}$$

The ratio (C.7) contains the time dilation Doppler shift factor $\cosh\lambda$, but also the additional factor π/y_+. This additional factor is always greater than 1, tending to 1 as $v \to 0$ and increasing monotonically to infinity as $v \to 1$.

C.2 Inertial drift in a thermal bath

We consider next a detector on the inertial trajectory

$$\mathsf{x}(\tau) = \big(\tau\cosh\lambda, \tau\sinh\lambda, 0, 0\big)\,, \tag{C.8}$$

where $\lambda > 0$ and τ is the proper time. This trajectory has the constant drift velocity $v = \tanh\lambda$ in the Lorentz-frame defined by the coordinates.

We now take the field to be in the thermal state at temperature $T > 0$ in the Lorentz-frame defined by the coordinates. With switch-on and switch-off pushed to infinity, the transition rate is stationary, and it is obtained from (C.2) and (C.3) by first making the replacement

$$\begin{aligned}\frac{1}{(\Delta\mathsf{x})^2} &\to \sum_{n=-\infty}^{\infty} \frac{1}{-(\Delta t + in/T)^2 + (\Delta\mathbf{x})^2} \\ &= \frac{\pi T \sinh(2\pi T|\Delta\mathbf{x}|)}{|\Delta\mathbf{x}|\big[\cosh(2\pi T|\Delta\mathbf{x}|) - \cosh(2\pi T\Delta t)\big]}\,,\end{aligned} \tag{C.9}$$

which replaces the Minkowski vacuum by the thermal state, and then substituting in the trajectory (C.8), with the outcome

$$\frac{1}{(\Delta\mathsf{x})^2} \to \frac{\pi T}{2s\sinh\lambda}\big[\coth(\pi\,\mathrm{e}^{\lambda}\,Ts) - \coth(\pi\,\mathrm{e}^{-\lambda}\,Ts)\big]\ . \tag{C.10}$$

Proceeding as in (C.4) and (C.5), and converting the integral into a sum of the residues in the upper half-plane, we find

$$\dot{\mathcal{F}}(E) = \frac{T}{4\pi\sinh\lambda}\ln\left(\frac{1-\exp(-\,\mathrm{e}^{\lambda}\,E/T)}{1-\exp(-\,\mathrm{e}^{-\lambda}\,E/T)}\right)\,, \tag{C.11}$$

as previously obtained in [44]. In the limit $\lambda \to 0$, (C.11) reduces to the Planckian formula $(2\pi)^{-1}E/\big(\mathrm{e}^{E/T}-1\big)$.

At $|E| \to \infty$, $\dot{\mathcal{F}}(E)$ (C.11) satisfies the KMS condition (5.7) at the temperature $T_{\mathrm{T+drift}} = \mathrm{e}^{\lambda}\,T$. Hence

$$\frac{T_{\mathrm{T+drift}}}{T} = \mathrm{e}^{\lambda}\ . \tag{C.12}$$

The ratio (C.12) is equal to the Doppler blueshift factor of the quanta that the detector sees head on from the direction of its motion, higher than the time dilation Doppler shift factor $\cosh\lambda$ that is experienced by the quanta seen from the directions transverse to the motion. The transition rate at large excitation energies is hence dominated by the most energetic, head-on quanta. (We thank Eric Poisson for this observation.) We note that the ratio (C.12) is not as large as the ratio (C.7).

C.3 Rotating detector in a thermal bath

We consider finally a rotating detector. The trajectory is

$$\mathsf{x}(\tau) = \big(\gamma\tau, R\cos(\gamma\Omega\tau), R\sin(\gamma\Omega\tau), 0\big)\,, \tag{C.13}$$

where $R > 0$, $0 < \Omega < 1/R$, $\gamma = (1 - R^2\Omega^2)^{-1/2}$, and τ is the proper time. The trajectory traces in space a circle of radius R, and the angular velocity in the adapted Lorentz frame is Ω. The trajectory is stationary, following an orbit of the Killing vector $\partial_t + \Omega(x\partial_y - y\partial_x)$. The proper acceleration is $R\gamma^2\Omega^2$.

We again take the field to be in the thermal state at temperature $T > 0$ in the Lorentz-frame defined by the coordinates. With switch-on and switch-off pushed to infinity, the transition rate is stationary, and it is obtained from (C.2) and (C.3) by the thermal replacement (C.9) and by substitution of the trajectory (C.13), with the outcome

$$\frac{1}{(\Delta\mathsf{x})^2} \to \frac{\pi T \sinh\big[4\pi T R \sin(\gamma\Omega s/2)\big]}{2R\sin(\gamma\Omega s/2)\left\{\cosh\big[4\pi T R\sin(\gamma\Omega s/2)\big] - \cosh(2\pi\gamma T s)\right\}}\,. \tag{C.14}$$

Proceeding as in (C.4) and (C.5), we find that the correction to the inertial Minkowski vacuum transition rate is given by

$$\dot{\mathcal{F}}^{\rm corr}(E) = \frac{T}{8\pi R\gamma\Omega}\int_C \frac{\exp\big[i2|E|z/(\gamma\Omega)\big]\sinh(4\pi T R\sin z)\,{\rm d}z}{\sin z\sinh\big[2\pi T(R\sin z + z/\Omega)\big]\sinh\big[2\pi T(R\sin z - z/\Omega)\big]}\,, \tag{C.15}$$

where we have introduced a new integration variable by $z = \gamma\Omega s/2$ and the contour C is along the real axis except for passing the pole at $z = 0$ in the upper half-plane. Note that the integrand in (C.15) is nonsingular on C since $R\Omega < 1$ and the $z \neq 0$ zeroes of $\sin z$ in the denominator coincide with simple zeroes in the numerator. A formula equivalent to (C.15) was obtained and analysed in certain limits in [44].

A standard set of contour deformation arguments again shows that the integral in (C.15) equals $2\pi i$ times the sum of the residues of the poles in the upper half-plane. The dominant contribution at $|E| \to \infty$ comes from the pole with the smallest imaginary part, and it can be shown that this pole is on the positive imaginary axis in z.

To identify the dominating pole, let ρ_+, ρ_- and $T_{\rm crit}$ be the unique positive

solutions to the transcendental equations

$$0 = \sinh \rho_+ - \frac{\rho_+}{R\Omega} \,, \tag{C.16a}$$

$$\frac{1}{2RT} = \sinh \rho_- + \frac{\rho_-}{R\Omega} \,, \tag{C.16b}$$

$$R\Omega = 4RT_{\text{crit}} \operatorname{arcsinh}\left(\frac{1}{4RT_{\text{crit}}}\right) . \tag{C.16c}$$

With this notation, the dominating pole is at $z = i\rho_+$ when $T < T_{\text{crit}}$ and at $z = i\rho_-$ when $T > T_{\text{crit}}$. From (C.15), we hence have

$$\dot{\mathcal{F}}^{\text{corr}}(E) \sim \frac{\exp\bigl[-2|E|\rho_\pm/(\gamma\Omega)\bigr]}{8\pi R\gamma \sinh\rho_\pm \, (R\Omega\cosh\rho_\pm \mp 1)} \,, \qquad |E| \to \infty \,, \tag{C.17}$$

where the upper sign applies for $T < T_{\text{crit}}$ and the lower sign applies for $T > T_{\text{crit}}$. When $T = T_{\text{crit}}$, the two simple poles merge into a dominating second-order pole, and the exponential factor in (C.17) continues to hold but the pre-exponential factor gets modified.

From (C.2), (C.3a) and (C.17) it follows that $\dot{\mathcal{F}}(E)$ satisfies at $|E| \to \infty$ the KMS condition (5.7) at the temperature

$$T_{\text{rot}} = \begin{cases} \dfrac{\gamma\Omega}{2\rho_+} & \text{for } T < T_{\text{crit}} \,, \\[2ex] \dfrac{\gamma\Omega}{2\rho_-} & \text{for } T > T_{\text{crit}} \,. \end{cases} \tag{C.18}$$

In the low temperature regime, $T < T_{\text{crit}}$, T_{rot} is independent of T: in this regime, T_{rot} is fully determined by the acceleration and does not feel the ambient temperature. In the high temperature regime, $T > T_{\text{crit}}$, by contrast, T_{rot} depends on both T and Ω. A plot of T_{rot} as a function of Ω and T is shown in Figure 14.

We note from (C.16) and (C.18) that RT_{rot} is dimensionless and depends only on the dimensionless combinations $R\Omega$ and RT. This means that R enters the relations between T_{rot}, Ω and T only as an overall scale. The system can be parametrised by the three independent positive parameters

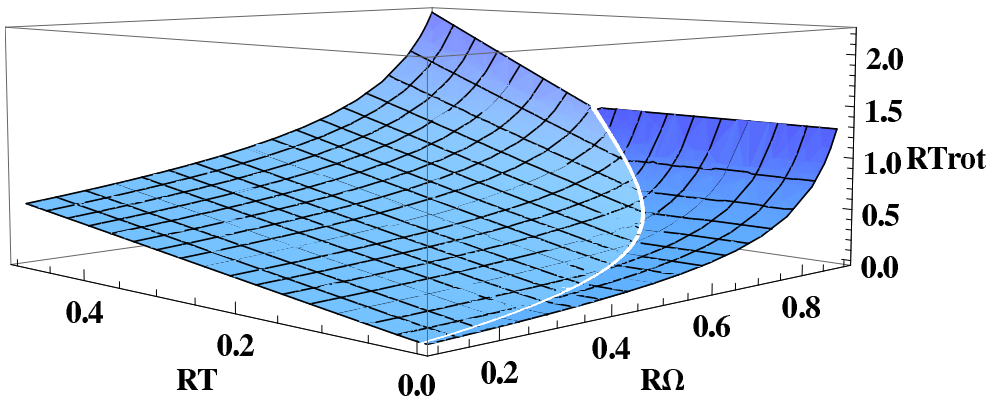

Figure 14: The rotating detector's asymptotic temperature $T_{\rm rot}$ (C.18) is plotted as a function of the ambient temperature T and the detector's angular velocity Ω, all expressed in units of $1/R$, where R is the radius of the detector's orbit. In the low temperature regime $T_{\rm rot}$ is independent of T, and the transition between the low temperature regime and the high temperature regime is clearly visible in the plot. The limit $\Omega \to 0$ at fixed T is in the high temperature regime and gives $T_{\rm rot} \to T$, visible in the plot as the straight line at $\Omega = 0$: this is the familiar result for an inertial detector in a co-moving thermal bath.

(R, ρ_+, ρ_-), in terms of which we have

$$R\Omega = \frac{\rho_+}{\sinh \rho_+}\,, \tag{C.19a}$$

$$RT = \frac{1}{2\left(\sinh \rho_- + \rho_- \rho_+^{-1} \sinh \rho_+\right)}\,, \tag{C.19b}$$

$$RT_{\rm crit} = \frac{1}{4 \sinh \rho_+}\,, \tag{C.19c}$$

$$RT_{\rm rot} = \begin{cases} \dfrac{1}{2\sqrt{\sinh^2 \rho_+ - \rho_+^2}} & \text{for } \rho_- > \rho_+ \quad (T < T_{\rm crit})\,, \\ \dfrac{\rho_+}{2\rho_- \sqrt{\sinh^2 \rho_+ - \rho_+^2}} & \text{for } \rho_- < \rho_+ \quad (T > T_{\rm crit})\,, \end{cases} \tag{C.19d}$$

where the low temperature regime $T < T_{\rm crit}$ occurs for $\rho_- > \rho_+$ and the high temperature regime $T > T_{\rm crit}$ occurs for $\rho_- < \rho_+$.

We wish to compare $T_{\rm rot}$ to the ambient temperature T. From (C.18)

and (C.19), we have

$$\frac{T_{\rm rot}}{T} = \begin{cases} \gamma\left(\dfrac{\rho_-}{\rho_+} + \dfrac{\sinh\rho_-}{\sinh\rho_+}\right) & \text{for } \rho_- > \rho_+ \quad (T < T_{\rm crit})\,, \\ \gamma\left(1 + \dfrac{\rho_+\sinh\rho_-}{\rho_-\sinh\rho_+}\right) & \text{for } \rho_- < \rho_+ \quad (T > T_{\rm crit})\,. \end{cases} \tag{C.20}$$

The ratio (C.20) contains the expected time dilation Doppler shift factor γ, but also an additional factor that is always greater than unity, taking values in the interval $(1, 2)$ in the high temperature regime and in the half-line $(2, \infty)$ in the low temperature regime. Note that this additional factor depends not just on the detector's trajectory but also on T, even in the high-temperature regime $T > T_{\rm crit}$.

As a final observation, we consider the limit $T \to 0$, in which the field is in the Minkowski vacuum, and we compare $T_{\rm rot}$ to the Unruh temperature of a Rindler trajectory with the same value of proper acceleration, $T_{\rm Rindler} = R\gamma^2\Omega^2/(2\pi)$. From (C.19), we obtain

$$\left.\frac{T_{\rm rot}}{T_{\rm Rindler}}\right|_{T=0} = \frac{\pi\sqrt{\sinh^2\rho_+ - \rho_+^2}}{\rho_+^2}\,, \tag{C.21}$$

where ρ_+ is determined by $R\Omega$ from (C.19a). The ratio (C.21) takes values on the half-line $(\pi/\sqrt{3}, \infty)$, asymptoting to $\pi/\sqrt{3}$ in the ultrarelativistic limit $R\Omega \to 1$ and to ∞ in the inertial limit $R\Omega \to 0$. This disagreement between $T_{\rm rot}$ and $T_{\rm Rindler}$ highlights the qualitative differences between linear acceleration and circular acceleration in Minkowski vacuum [3, 4, 6].

References

[1] W. G. Unruh, Phys. Rev. D **14**, 870 (1976).

[2] B. S. DeWitt, "Quantum gravity: the new synthesis", in *General Relativity; an Einstein centenary survey* ed S. W. Hawking and W. Israel (Cambridge University Press, 1979) 680.

[3] J. R. Letaw, Phys. Rev. D **23**, 1709 (1981).

[4] P. G. Grove and A. C. Ottewill, J. Phys. A **16**, 3905 (1983).

[5] S. Takagi, Prog. Theor. Phys. Suppl. **88**, 1 (1986).

[6] D. Müller, gr-qc/9512038.

[7] L. C. B. Crispino, A. Higuchi and G. E. A. Matsas, Rev. Mod. Phys. **80**, 787 (2008) [arXiv:0710.5373 [gr-qc]].

[8] J. B. Hartle and S. W. Hawking, Phys. Rev. D **13**, 2188 (1976).

[9] W. Israel, Phys. Lett. A **57**, 107 (1976).

[10] G. W. Gibbons and S. W. Hawking, Phys. Rev. D **15**, 2738 (1977).

[11] L. Hodgkinson and J. Louko, Phys. Rev. D **86** (2012) 064031 [arXiv:1206.2055 [gr-qc]].

[12] J. Louko and A. Satz, Class. Quant. Grav. **23**, 6321 (2006) [arXiv:gr-qc/0606067].

[13] A. Satz, Class. Quant. Grav. **24**, 1719 (2007) [arXiv:gr-qc/0611067].

[14] J. Louko and A. Satz, Class. Quant. Grav. **25**, 055012 (2008) [arXiv:gr-qc/0710.5671].

[15] L. Hodgkinson and J. Louko, J. Math. Phys. **53**, 082301 (2012) [arXiv:1109.4377 [gr-qc]].

[16] B. S. Kay and R. M. Wald, Phys. Rept. **207**, 49 (1991).

[17] Y. Décanini and A. Folacci, Phys. Rev. D **73**, 044027 (2006) [arXiv:gr-qc/0511115].

[18] C. J. Fewster, Class. Quant. Grav. **17**, 1897 (2000) [arXiv:gr-qc/9910060].

[19] W. Junker and E. Schrohe, Ann. Henri Poincaré **3**, 1113 (2002) [arXiv:math-ph/0109010].

[20] L. Hörmander, *The Analysis of Linear Partial Differential Operators I (Distribution Theory and Fourier Analysis)*, 2nd Edition (Springer, Berlin, 1990), Theorem 8.2.4.

[21] L. Hörmander, "Fourier Integral Operators. I", Acta Mathematica **127**, 79 (1971), Theorem 2.5.11'. Reprinted in: J. Brüning and V. W. Guillemin (Editors), *Fourier Integral Operators* (Springer, Berlin, 1994).

[22] N. D. Birrell and P. C. W. Davies, *Quantum Fields in Curved Space* (Cambridge University Press 1982).

[23] R. Kubo, J. Phys. Soc. Jap. **12**, 570 (1957).

[24] P. C. Martin and J. S. Schwinger, Phys. Rev. **115**, 1342 (1959).

[25] R. C. Tolman and P. Ehrenfest, Phys. Rev. **36**, 1791 (1930)

[26] S. W. Hawking, Commun. Math. Phys. **43**, 199 (1975) [Erratum-ibid. **46**, 206 (1976)].

[27] A. Ottewill and S. Takagi, Prog. Theor. Phys. **77**, 310 (1987).

[28] M. Smerlak and S. Singh, Phys. Rev. D **88**, 104023 (2013) [arXiv:1304.2858 [gr-qc]].

[29] R. M. Wald, *Quantum field theory in curved spacetime and black hole thermodynamics* (University of Chicago Press, Chicago, 1994).

[30] Wolfram Research, Inc., Mathematica, Version 8.0, Champaign, Illinois (2010).

[31] E. W. Leaver, J. Math. Phys. **27**, 1238 (1986).

[32] S. M. Christensen and S. A. Fulling, Phys. Rev. D **15**, 2088 (1977).

[33] "NIST Digital Library of Mathematical Functions," *http://dlmf.nist.gov/*

[34] P. Candelas, Phys. Rev. D **21**, 2185 (1980).

[35] S. Abdolrahimi, [arXiv:1304.4237 [gr-qc]].

[36] L. C. Barbado, C. Barcelo, L. J. Garay, Class. Quant. Grav. **28**, 125021 (2011) [arXiv:1101.4382 [gr-qc]].

[37] L. Hodgkinson, "Particle detectors in curved spacetime quantum field theory", PhD Thesis, University of Nottingham (2013) [arXiv:1309.7281 [gr-qc]].

[38] D. N. Page, Phys. Rev. D **13**, 198 (1976).

[39] B. P. Jensen, J. G. McLaughlin and A. C. Ottewill, Phys. Rev. D **45**, 3002 (1992).

[40] P. Langlois, Annals Phys. **321**, 2027 (2006) [arXiv:gr-qc/0510049].

[41] H. Nariai, Sci. Rep. Tohoku Univ. **34**, 160 (1950).

[42] H. Nariai, Sci. Rep. Tohoku Univ. **35**, 62 (1951).

[43] H. Kleinert, *Path Integrals in Quantum Mechanics, Statistics, Polymer Physics, and Financial Markets*, 5th edition (World Scientific, Singapore 2009).

[44] S. S. Costa and G. E. A. Matsas, Phys. Rev. D **52**, 3466 (1995).